CHALMERS
UNIVERSITY OF TECHNOLOGY

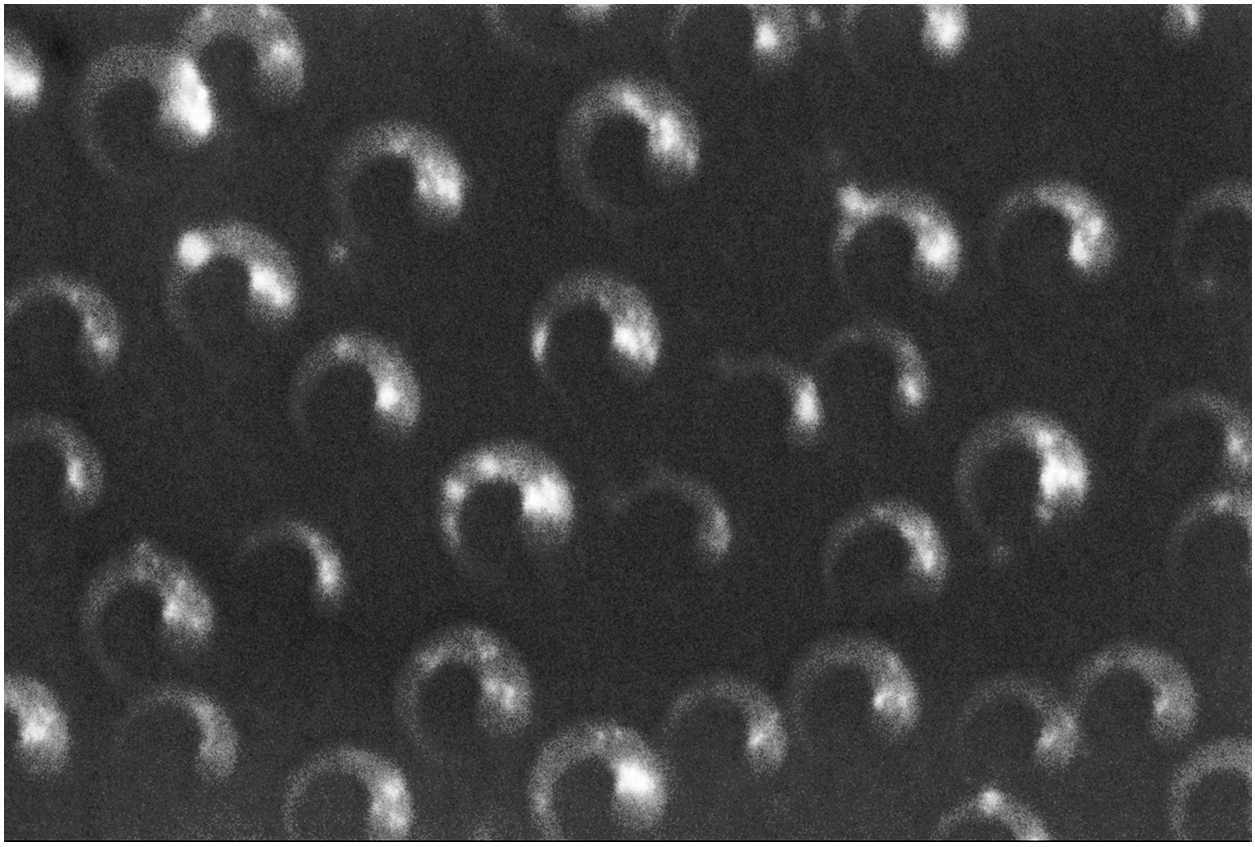

Nano-optical Control of Chiral Photochemistry

Master's thesis in Nanotechnology

WERA LARSSON

Department of Physics
CHALMERS UNIVERSITY OF TECHNOLOGY
Gothenburg, Sweden 2019

Master's thesis 2019

Nano-optical Control of Chiral Photochemistry

WERA LARSSON

CHALMERS
UNIVERSITY OF TECHNOLOGY

Department of Physics
Chalmers University of Technology
Gothenburg, Sweden 2019

Nano-optical Control of Chiral Photochemistry
WERA LARSSON

Supervisor: Esteban Pedrueza Villalmanzo, Department of Physics, University of Gothenburg
Examiner: Alexander Dmitriev, Department of Physics, University of Gothenburg

Master's Thesis 2019
Department of Physics
Chalmers University of Technology
SE-412 96 Gothenburg
Telephone +46 31 772 1000

Cover: SEM micrograph of spiral shaped aluminium nanoantennas that are used for chiral synthesis.

Gothenburg, Sweden 2019

Nano-optical Control of Chiral Photochemistry
WERA LARSSON
Department of Physics
Chalmers University of Technology

Abstract

Many active compounds in pharmaceutical drugs are chiral, meaning that they consist of molecular forms that cannot be superimposed into one another. The different chiral forms are called enantiomers, and the pharmaceutical properties of the different enantiomers can vary extensively. One of the major challenges within the pharmaceutical industry when it comes to cost-effective manufacturing of safe and effective pharmaceutical drugs is therefore to produce medicines consisting of only one enantiomer, so called enantiopure compounds. Today, the chiral synthesis of enantiopure compounds is mainly done by using complicated and expensive methods within advanced organic chemistry. This thesis proposes a new physical approach to chiral synthesis, which is both cheaper and less complicated compared to the methods used today.

In order to test this approach, a model system based on the chiral photochemical reaction of a model prochiral molecular photoswitch is used. The photoswitch is a derivative of dithienylethene (DTE) called DTE-1, and it undergoes a reversible phototransformation between an achiral and a chiral form commonly called the 'open' and 'closed' forms respectively. The two enantiomers in the closed form have a different ability for absorbing left and right circularly polarized light (LCP and RCP light), but this difference is most often not enough to create a considerable enantiomeric excess of one or the other enantiomers by only illuminating them with LCP or RCP light. Optical plasmonic nanoantennas, which are antennas that can manipulate (i.e. receive and transmit, modify its polarization etc.) light on the nanoscale, are designed and fabricated to have an enhanced chiral optical near-field. Experimental characterization methods involving circular dichroism (CD) spectroscopy has together with numerical simulations indicated that the fabricated nanoantennas have the desired properties.

By placing the DTE-1 molecules in a close proximity of the nanoantennas and illuminating with non-polarized light of the wavelengths that trigger the photochemical reaction, the aim is for the enhanced near-field to induce an enantiomeric excess at phototransformation. According to the results presented in this thesis, this is achieved for two samples made up of spiral shaped aluminium nanoantennas. Reproducibility of both the fabrication and chiral synthesis was not possible to prove within the time frame of this thesis, and is something that needs to be considered in order to draw final conclusions. Even though there still is an extensive amount of work needed before the proposed approach could be used within the pharmaceutical drug development process, this thesis paves the way towards this vision.

Keywords: pharmaceutical drugs, chirality, enantiomers, chiral synthesis, DTE-1, plasmonic nanoantennas, near-field enhancement, circular dichroism

Acknowledgements

During the course of this master's thesis work, I have truly learnt that research is a collaborative effort and this thesis would not have been possible without the help and support from many people. First of all, I would like to thank my supervisor Dr. Esteban Pedrueza Villalmanzo who has been an invaluable source of knowledge and ideas throughout this project. I am very grateful for all the time and effort you have put into helping me and giving me valuable feedback to help steering me in the right direction.

I would also like to thank my examiner and group leader Prof. Alexander Dmitriev who gave me the chance to be part of his research group and to take on this very exciting thesis project. I am grateful for the insightful discussions and feedback along the course of my work. Sincere gratitude also goes out to the rest of the Dmitriev group, especially Dr. Evgeniya Smetanina who has been a tremendous help during the computational work. I am grateful for the help from Prof. Joakim Andreasson who has been a huge source of information, and who has given me a lot of support regarding the chemistry related parts of the thesis. A big thank you to the many lab technicians working in the MC2 cleanroom, for providing training and immense knowledge of the tools and processes I have used there. A special mention of Dr. Henrik Fredriksson for helping me realize my nanoantennas.

Finally, I would like to thank my wonderful family, friends and boyfriend for their endless support, encouragements and for always being there for me. I cannot thank you enough.

Wera Larsson, Gothenburg, June 2019

Contents

List of Figures

Abbreviations

AFM	Atomic Force Microscopy
CD	Circular Dichroism
DI	Deionized
DTE	Dithienylethene
EBL	Electron-beam lithography
FDTD	Finite-difference time-domain
HCL	Hole-mask colloidal lithography
LCP	Left circularly polarized
LD	Linear Dichroism
LSP	Localized surface plasmon
LSPR	Localized surface plasmon resonance
NP	Nanoparticle
PDDA	Polydiallyldimethylammonium chloride
PMMA	Polymethyl methacrylate
PS	Polystyrene
PVD	Physical vapor deposition
RCP	Right circularly polarized
RIE	Reactive ion etching
SEM	Scanning Electron Microscopy
SP	Surface plasmon
SPM	Scanning Probe Microscopy
SPP	Surface plasmon polariton
THF	Tetrahydrofuran
UV	Ultraviolet

1
Introduction

Cost-efficient development of safe and effective pharmaceutical drugs is of essential importance when it comes to treating diseases, and hence is a vital task for biomedical industries and researchers worldwide. One of the major challenges in the pharmaceutical industry when it comes to this is the task of obtaining enantiopure compounds, meaning that they consist only of molecules of one chiral form [1]. Chirality is a type of asymmetry, in which a chiral object is an object that is not superimposable onto its mirror image. Molecules of different chiral forms are called enantiomers [2], and the challenge in the pharmaceutical industry is therefore to make compounds consisting of only one enantiomer. Based on the chirality of the molecule, the pharmaceutical properties can vary extensively. In some cases, one enantiomer of the active compound in the medicine might cure the patient from the disease while the other one could be either inactive, antagonizing the curing effect of the other enantiomer or be toxic. One of the most known examples of this is thalidomide, which was a drug that was used by pregnant women to prevent morning sickness in the middle of the 20th century. This resulted in thousands of children being born with malformed limbs. In the case of thalidomide only one of the enantiomers is in fact harmful, but the conversion between the two enantiomers can take place inside the human body making both enantiomers effectively harmful.

Pharmaceuticals consisting of equal amounts of the left- and right-handed enantiomers of a chiral molecule, a so called racemic mixture or racemate, are possibly less effective and safe as medicines compared to enantiopure compounds due to the difference in pharmaceutical properties between different enantiomers. Chemical separation of different enantiomers is both difficult and costly, which is mainly due to the physical properties being the same for the different enantiomers [3][4]. Today, controlling the chiral synthesis and in that way obtaining enantiopure compounds is mainly done by using advanced organic chemistry, which is both complicated and expensive. In this thesis a new physical approach to chiral synthesis is proposed instead, which could potentially solve the issue of obtaining enantiopure compounds in a cost-efficient way.

Here we study a model system based on a chiral photochemical reaction. The molecules that will be used for the chiral synthesis are a derivative of dithienylethene (DTE) called DTE-1. They can be seen as model prochiral molecular photoswitches [5], meaning that they phototransform between the achiral and chiral forms in one step. The transformation is reversible, and the forms are often mentioned as the

'open' and the 'closed' forms. In the open form, the chirality of DTE-1 changes continuously between the enantiomers, resulting in a compound that is always achiral. The chiral structure is fixed in the closed form, and consists of two enantiomers. Transformation of the DTE derivative from the open form into the closed form occurs when they absorb ultraviolet (UV) light, and the reverse isomerization is triggered by light in the visible spectral region. The goal here is to achieve a non-racemic mixture, or a so called enantiomeric excess, of the molecules in the closed form and controlling this using nano-optics.

In order to do this, optical plasmonic nanoantennas are designed to have a structural and/or electromagnetic chirality, and thus enhanced chiral optical near-field. A plasmonic nanoantenna is a nanoscaled metallic structure that can manipulate light on the nanoscale, analogously to how a conventional radio antenna can manipulate electromagnetic waves at longer wavelengths. By enhancing the electrical near-fields surrounding the nanoantennas, the molecules in a direct proximity to the nanoantennas can be affected as well. The nanoantennas are fabricated using the versatile and fairly simple bottom-up nanofabrication method of hole-mask colloidal lithography (HCL) [6], that makes it possible to fabricate samples on the cm^2 scale. By measuring the far-field circular dichroism (CD) of the structures, the chirality of the antennas in this project can be predicted and these results are compared to numerical simulations of single nanoantennas. In this project the nanoantennas are made of aluminium, with a goal of combining noble metals and metallic ferromagnetic elements in future developments where the optical near-field of such nanoantennas can be modified by the externally applied milli-Tesla magnetic fields. By placing the molecular photoswitches in the direct proximity of these plasmonic nanoantennas, the goal is to try to enhance the possibility of achieving an excess of one or the other enantiomers and hence control the chiral synthesis.

1.1 Aim

The aim of this thesis is to develop a nano-optical control of the chiral photochemical isomerization of DTE-1. By doing this, the results can hopefully pave the way for a completely new physical approach to control chiral synthesis at the nanoscale using magnetic fields.

1.2 Limitations

This thesis focuses on controlling the chiral synthesis of one specific DTE derivative (DTE-1), excluding other chiral photochemical reactions or other chiral chemical reactions in general. The quantity of the enantiomeric excess is not determined. Regarding the fabrication of the nanoantennas, the method used in this thesis is

limited to hole-mask colloidal lithography and only structures made of aluminium deposited on quartz are produced and characterized.

1.3 Specification of issue under investigation

In order to achieve the aim of the thesis, the following questions will need to be answered during the course of the project:

- How can different shapes of aluminium nanoantennas be fabricated?
- How much far-field CD can be achieved at the desired wavelengths by the nanoantennas?
- What is the numerically calculated near-field CD for the single nanoantennas?
- How well does the experimentally measured far-field enhancement coincide with the numerically calculated near-field enhancements?
- Is it possible to control the isomerization of DTE-1 with the fabricated nanoantennas and is the possibly achieved enantiomeric excess measurable?

1.4 Thesis outline

This thesis consists of five chapters:

Chapter 2: This chapter presents the theoretical background needed to understand the thesis work. This includes the theory behind plasmonics, chirality, linear and circular dichroism, and also background regarding different material choices and the photoinduced chemical reaction.

Chapter 3: This chapter describes the various methods used in the thesis, including fabrication of the nanoantennas, numerical electromagnetic calculations, characterization techniques and the experimental setup used to combine the structures and molecules in order to control the isomerization.

Chapter 4: The results of the thesis are presented, analysed and discussed in this chapter. They consist of experimentally measured far-field CD of the structures together with numerically calculated near-fields of single nanoantennas, and also results from the molecular tests. Possible error sources are also presented, together with discussions regarding the methods that have been used.

Chapter 5: The final chapter includes a summary of the work and results presented in the thesis, and a conclusion is drawn from the findings. A future outlook is also provided to present future research possibilities based on this thesis.

2

Theory

This chapter aims to present the theoretical background needed to understand and fully appreciate the results presented later in the thesis. Theory regarding plasmonics and chirality is first presented separately, and following this an introduction to chiral plasmonics/chirality on the nanoscale is given. It will also involve basic background regarding linear and circular dichroism, which is of great importance for understanding the methods used and when evaluating the results.

2.1 Plasmonics

Due to new phenomena arising on the nanoscale, metals has become much more of a material of choice when it comes to modern optical studies and more specifically nanophotonics [7]. The study of interactions between electromagnetic radiation and metals on the sub-wavelength scale via so-called surface plasmons is called plasmonics, and constitutes a major part of nanophotonics [8][9]. Even though the word plasmonics and the fundamental understanding of the processes involved did not emerge until much later, this field actually dates back two thousand years to the Medieval and Roman era [10]. During this time, metal nanoparticles (NPs) were used to stain glass for windows and ornaments like the famous Lycurgus cup shown in Figure 2.1 [11]. The latter is a Roman-era cup made of glass that contains small amounts of gold particles similar in size to the wavelengths of visible light. When a light source is placed outside the cup, the color is green primarily due to reflection, and when it is placed inside the cup, it turns red due to absorption and transmission.

It was not until the middle of the 19th century that Michael Faraday performed the first ever systematic studies of the light and matter interactions [9]. His findings paved the way for many more scientists to come, and today the phenomena used in ancient applications can be explained. When metal particles are downsized to match the wavelength of light, the interactions between light and matter changes dramatically in the sense of reflection, scattering and absorption of colors. Today it is known that the properties change with size, shape and arrangement of the

NPs.

(a) Lycurgus cup illuminated from outside.

(b) Lycurgus cup illuminated from inside.

Figure 2.1: Image showing the iconic Lycurgus cup illuminated from the outside and inside. Taken from [11].

2.1.1 Surface plasmons

The phenomena studied within the field of plasmonics is that of surface plasmons (SPs), which are plasma-like oscillations propagating along a conductor surface [12]. They consist of free electrons oscillating resonantly with the incoming electromagnetic waves, and are localized on the surface of the interface of a metal and a dielectric (e.g. the surrounding air). SPs can be either propagating in the form of surface plasmon polaritons (SPPs) or non-propagating in the form of localized surface plasmons (LSPs) [7].

2.1.2 Plasmonic nanoantennas

Localized surface plasmon resonances (LSPRs) are highly confined SPs, arising when sub-wavelength sized NPs are excited by electromagnetic waves [13]. These resonances make the NPs function as light capturing nanoantennas [2]. In the same way as conventional low-frequency antennas can convert incoming micro- and radio frequency waves to current or radiate them, optical nanoantennas work with

light. Hence, the fundamental phenomena is the same, with the difference being the size of the antennas and thereby the frequency of the electromagnetic waves that are controlled by them. At the wavelengths that correspond to the LSPRs, the nanoantennas display intense absorption and scattering of light [13]. The electric near-fields are also enhanced, which in turn can cause enhanced absorption and emission of light by surrounding molecules.

2.1.3 Aluminium plasmonics

The most commonly used plasmonic materials are gold and silver, due to convenient properties like high free-electron carrier density that gives rise to higher quality plasmonic resonances in the sense of longer lifetime and lower damping which in turn results in higher light extinction efficiencies [14]. Gold is for example very resistant to oxidation and degradation, while silver shows very intense and narrow LSPRs. Both of these metals exhibit plasmonic properties in the visible and near-infrared spectral regions, but due to optical losses to the interband transitions they do not extend into the UV [15]. In order to reach also the high frequency side of the electromagnetic spectra, aluminium has become a promising material. Some of the properties that makes it a good candidate for UV-Vis plasmonics is that it has a high plasma frequency, high abundance, low cost and is also easily manipulated and stable due to the formation of a protective oxide layer at the surface [14][15]. One of the drawbacks is discrepancies between experimental and calculated optical response, with one of the explanations being that the optical properties of aluminium are quite sensitive to the amount of oxides and impurities. Its plasmonic properties and other advantages still makes it a promising material for practical applications [15].

2.2 Chirality

Chirality can be seen in almost all aspects of life, ranging from fundamental nuclear particles, proteins and DNA to the macroscopic world of plants and animals [2][16]. A chiral object is an object that cannot be superimposed into its mirror image, while an achiral object is superimposable with its mirror image. This is visualized in Figure 2.2 [17], where human hands are used as an example of chiral objects. The two chiral forms of a molecule are described as having left and right handedness, and the different chiral forms are called enantiomers [2]. Commonly used notations for the right- and left-handed enantiomers are *D* and *L*-enantiomers, or *R*- and *S*-enantiomers. A compound consisting of equal amounts of the two enantiomers is said to be a racemic mixture or a racemate, and when there is more of one or the other enantiomer it is called an enantiomeric excess.

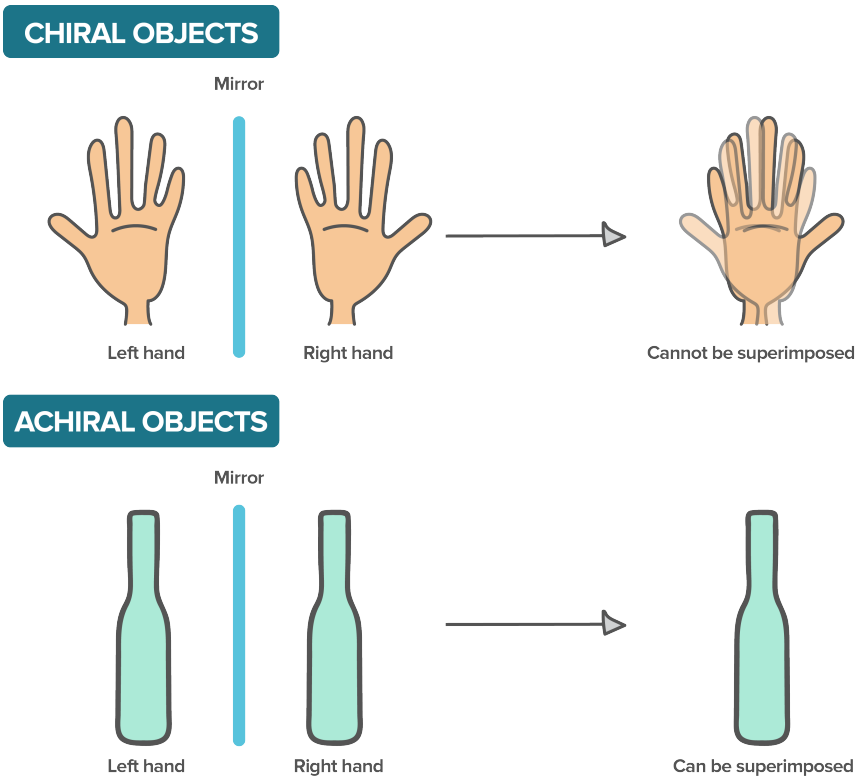

Figure 2.2: Figure showing the difference between chiral objects (objects that cannot be superimposed) and achiral objects (objects that can be superimposed). Taken from [17].

2.2.1 Chiroptical effects

Light can have different polarizations, and is said to be circularly polarized when the vector of the electric field **E** has a constant amplitude, but rotates continuously perpendicular to the wave propagation direction [18]. Circularly polarized light is commonly divided into right circularly polarized (RCP) and left circularly polarized (LCP) light, which corresponds to when the electric field is rotating clockwise or counter-clockwise respectively, when propagating towards the observer. A schematic figure visualizing RCP light can be seen in Figure 2.3 [19]. Linearly polarized light is composed by superposition of equal amplitudes of LCP and RCP light.

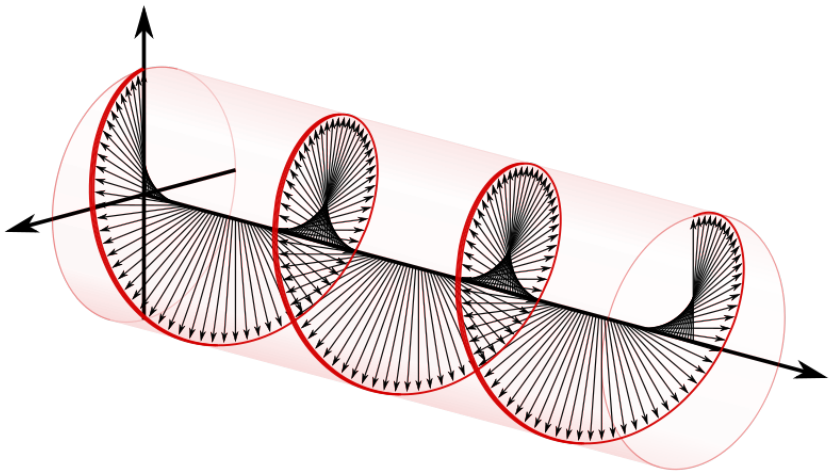

Figure 2.3: Figure showing right circularly polarized (RCP) light. The smaller arrows show the direction of the electric field **E** at different points of time. The propagation of the wave is along the long axis around which the light circulates. Taken from [19].

The difference in absorption of LCP and RCP is defined as circular dichroism (CD), and the definition is given in (2.1) [20]

$$CD = A_{LCP} - A_{RCP} \tag{2.1}$$

Chiral materials are hence materials that interact with RCP and LCP light differently [2]. This difference in the interaction with light of different handedness is wavelength dependent, and CD is therefore often measured spectrally. CD measurements can be used both in investigating the chirality of a structure, but also when investigating the enantiomeric excess of a molecular compound. A racemic mixture will in theory have no CD, while an enantiomeric excess will result in a positive or negative shift in the CD depending on which enantiomer is in majority. The CD response obtained when using a CD spectrometer is often obtained using the transmission of the LCP and RCP light through the medium, and can be expressed as in (2.2)

$$CD = \frac{T_{RCP} - T_{LCP}}{T_{RCP} + T_{LCP}} \tag{2.2}$$

Linear dichroism (LD) is the linear counterpart to CD, defined as the difference in absorption of parallel $\parallel$ and perpendicular $\perp$ linearly polarized light as shown in (2.3)

$$LD = A_{\parallel} - A_{\perp} \tag{2.3}$$

2.2.2 DTE-1 and chirality

Photoinduced reactions are reactions induced by light, and the reversible photoinduced transformation of two forms of a chemical species with different absorption spectra is called photochromism [21]. The photochromic molecule or photoswitch studied in this thesis belongs to a class of photochromic molecules called diarylethenes and are derivatives of stilbene. These compounds are thermally irreversible, resistant to fatigue (i.e. resistant to degradation due to repeated cycling between the stable states), have a high sensitivity, rapid response and can undergo the isomerization in solid state [21][22]. Equipped with these properties, diarylethenes make good candidates for several applications including the study made in this thesis.

The diarylethene used in this thesis is a derivative of dithienylethene, symmetrically substituted with methylpyridinium [5]. It is called DTE-1, and the structure can be seen in Figure 2.4. In the open form, DTE-1 is achiral due to a continuous shift between the two enantiomers. When irradiating the open form with UV light, the compound isomerizes to the closed form. The closed form consists of two enantiomers, that naturally exist in a racemic mixture. Visible light is used to trigger the reverse isomerization back to the open form. Figure 2.5 shows the absorption spectra of the open and closed forms of DTE-1, when the compound is dissolved in THF (0.02 mg/ml DTE-1/THF). From these spectra it is evident that the open form only absorbs in the UV and that the closed forms are the only ones absorbing in the visible part of the spectra, which explains why UV and visible light triggers the forward and reverse isomerization of DTE-1. The two enantiomers have opposite preferential absorption regarding LCP and RCP light, but due to the preferential difference being quite small enantiomeric separation only using either LCP or RCP light is only effective to a few percent [4].

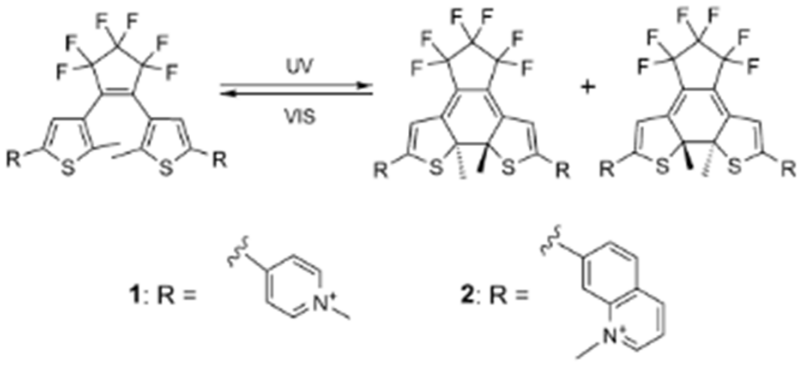

Figure 2.4: Figure showing the reversible photochromic isomerization of DTE, with the functional group, R, denoted as **1** representing the DTE-1 derivative of DTE. The achiral open form is shown to the left, and the two closed form enantiomers are shown to the right. Taken from [5].

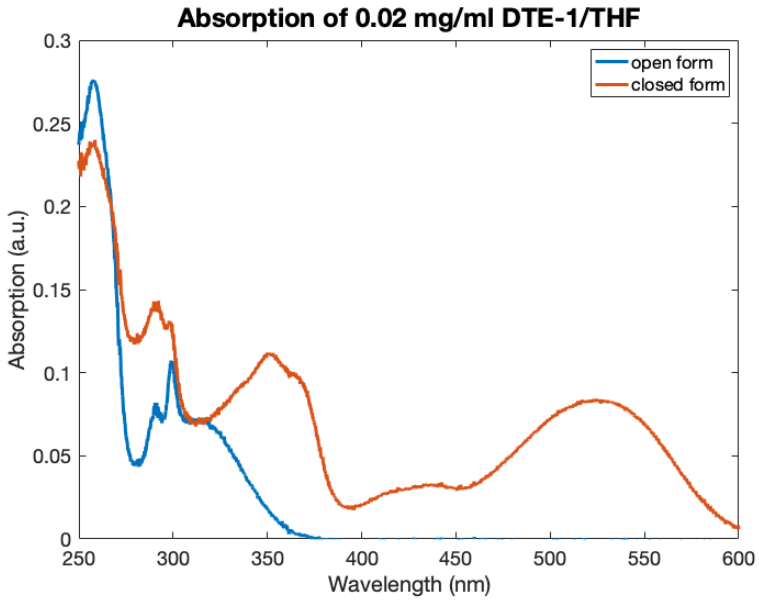

Figure 2.5: Figure showing the absorption spectra of the open and closed forms of DTE-1. The open form only absorbs in the UV, while the closed forms are the only ones absorbing in the visible part of the spectra. This explains why UV and visible light triggers the forward and reverse isomerization, respectively.

2.3 Chiral plasmonics

When exploring chirality on the nanoscale, there is a growing interest in creating chiral materials based on plasmonic nanostructures. Chiroptical effects can be strongly enhanced by plasmonics via confinement of incoming electromagnetic waves and enhancement of near-fields, making chiral plasmonic structures good candidates for various applications [23]. These applications include chiral catalysis, sensing and novel optical devices [20]. The chirality of the plasmonic nanostructures arise either intrinsically from asymmetry in the structures or arrangement of them, or extrinsically from the mutual arrangement of non-chiral structures and the incoming electromagnetic waves [2].

Enhancing chiroptical effects, and specifically CD by designing and fabricating chiral plasmonic structures, has been the aim of many recent studies [24][25]. It has been shown that it is possible to both achieve giant CD responses and also to tune the chiroptical effects [26][27]. The nanoantennas used can have either 2D or 3D chiral structures, or even have an achiral structure but make use of material asymmetry [2]. This gives almost endless possibilities in the design of chiral plasmonic nanoantennas, with the possibility to tune the parameters in order to fit the desired application. With versatile nanofabrication methods at hand, many of these nanoantennas can also be fabricated and experimentally characterized and used in studies like this thesis.

3

Methods

In this chapter, the different methods used in order to achieve the aim of the thesis are presented. It is an extensive study, with the work being done spanning several different techniques and methods. This chapter has therefore been divided into five main sections: fabrication of samples, optical characterization of samples, imaging techniques, simulations and chiral synthesis.

3.1 Fabrication of samples

As mentioned in Chapter 1, the nanofabrication method used in this thesis is HCL. It is a versatile and widely used method that was developed at Chalmers University of Technology in 2007 as an improvement of existing colloidal lithography methods [6]. Compared to electron-beam lithography (EBL), HCL is both less time-consuming, cheaper and can be extended into larger substrates on the cm^2 scale in contrast to the limit of about μm^2 for EBL. The standard protocol used for the HCL fabrication of nanoantennas is visualized in Figure 3.1, and the steps are explained more in detail below. All of the nanofabrication was performed in the Nanofabrication Laboratory (MC2) at Chalmers.

Substrate preparation

Quartz was used as the substrate in this thesis, since it is UV transparent which is a property needed in the chiral synthesis. Organic compounds are generally photoactive in the UV spectral region, possibly making it a good substrate also in other similar studies. The dimensions of the quartz pieces were originally 25 mm x 25 mm x 1 mm, and during the fabrication they were sometimes cut into smaller pieces (halves or quarters). First, the quartz was cleaned in acetone using ultrasonication at full power for 3 min. After this, the substrates were dried and treated with oxygen O_2 plasma using reactive ion etching (RIE) (5 s, 50 W, 250 mTorr, 10 sccm O_2, PlasmaTherm BatchTop m/95). A 200 nm sacrificial layer of polymethyl methacrylate

(PMMA) (950 PMMA, 4% diluted in anisole) was spin-coated onto the quartz, with increased adhesion as a result of the O_2 plasma treatment. The PMMA covered samples were then baked in a convection oven at 180 °C for 10 min.

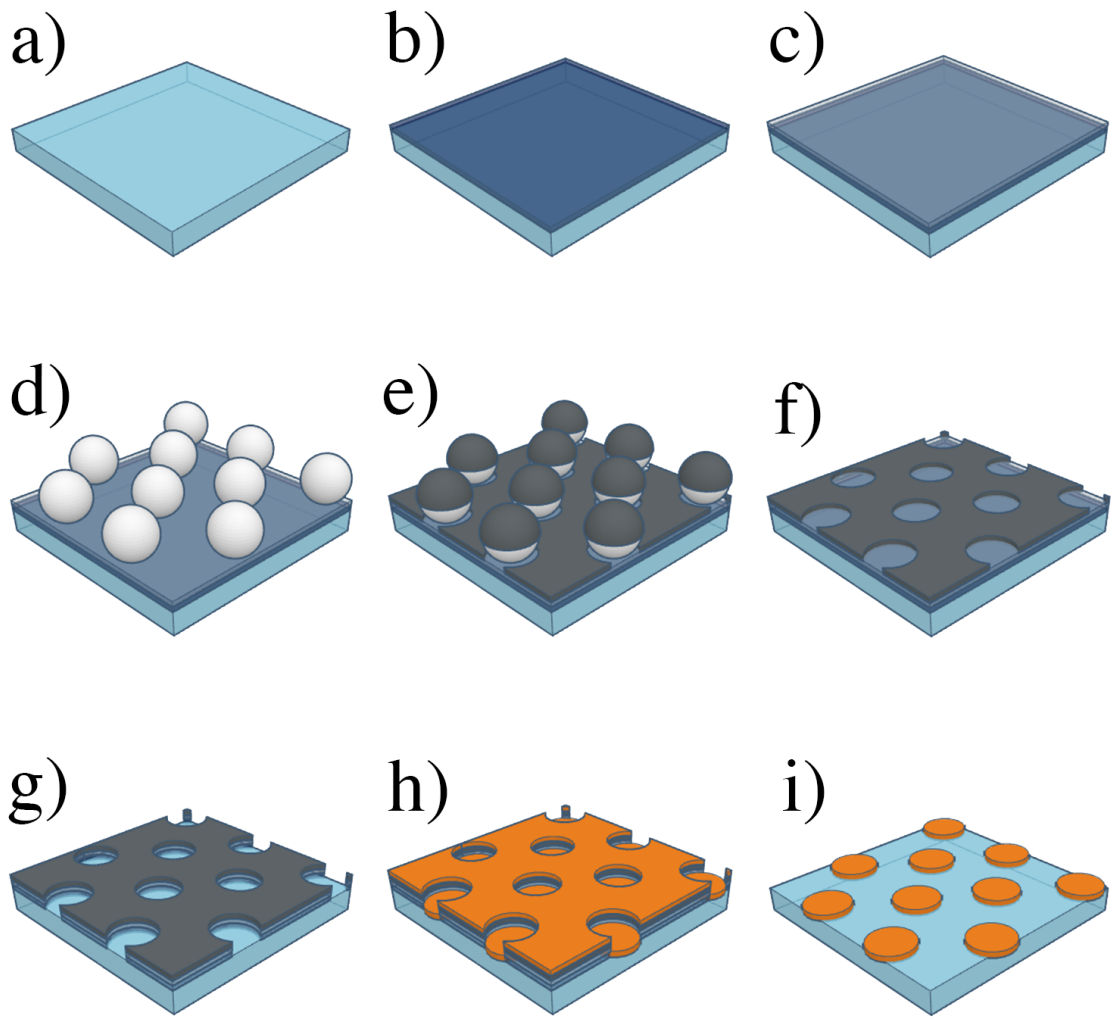

Figure 3.1: Schematic illustration of the HCL process: a) Cleaned quartz substrate is treated with O_2 plasma. b) PMMA is spin-coated onto the substrate and the sample is then baked and treated with O_2 plasma. c) A PDDA layer is applied on top of the PMMA. d) Polystyrene beads are deposited on top of the PDDA. e) Evaporation of a thin chromium mask. f) Tape-stripping of the polystyrene beads. g) O_2 plasma etch of PMMA layer through the nanoholes in the mask. h) Deposition of a metallic layer through evaporation. i) Lift-off in acetone leaving behind the nanoantennas on the quartz substrate.

Application of beads

In order to improve the hydrophilicity of the PMMA, the sample was once again etched in O_2 plasma for 5 s. After this, a 0.2vol% solution of positively charged polydiallyldimethylammonium chloride (PDDA) in deionized (DI) water was pipetted onto the hydrophilic PMMA surface and left for 1 min. The sample was then rinsed with DI water and dried using a nitrogen N_2 gun held perpendicular to the sample surface. A solution of negatively charged polystyrene (PS) beads (60 nm average diameter, 0.002-0.2wt% suspended in DI water) was then pipetted onto the PDDA layer and left for approximately 2 min. Electrostatic repulsion between the beads together with the opposite charges of the PDDA and the beads results in a random but uniform distribution of the beads, and the positively charged PDDA also improves the adhesion of the beads. The sample was then once again rinsed with DI water and dried in the same manner as before, in order to not remove or cause aggregation of the self-organized pattern of beads.

Mask deposition and etching of nanoholes

Physical vapor deposition (PVD) using an evaporator (Lesker PVD 225 #1) was used to deposit a 10 nm thin film layer of chromium on top of the samples. The deposition was done in a high vacuum chamber with pressures below 5×10^{-7} Torr, where electrons that are thermionically emitted and accelerated by a high voltage are focused towards a crucible containing the source material that is then vaporized and deposited onto the sample. After the deposition, the spheres were tape-stripped away leaving behind a plasma-resistant hole-mask in the chromium layer since the beads had blocked part of the chromium from reaching the substrate. RIE using O_2 plasma was then used to etch through the PMMA layer inside the nanoholes until the quartz was exposed for the next metal deposition. The etching was done for 7 min in order to create an undercut needed to make the desired nanoantennas. Too short etching times will result in the nanoantennas being deposited on PMMA instead of the quartz, and they will be lifted off together with the mask. Too long etching times might instead result in the mask falling off due to the supporting PMMA layer being completely removed. Apart from possible fabrication failures, the etching time is one of the parameters that can be changed depending on what structures are being fabricated.

Metal deposition and lift-off

The final deposition of the actual nanostructures was done using PVD evaporation (Lesker PVD 225 #2) at low pressure, just as for the mask deposition. The metal was deposited through the mask, and together with the etching step this is the part of the HCL process that can be altered in order to fabricate various sizes and

shapes of the nanostructures. By using different recipes and adjusting parameters like rotation speed, tilting angles and velocity, deposition height and stop angles, a huge versatility of nanostructures can be fabricated using the HCL fabrication method. More detailed descriptions will be given in the following sections on how the aluminium nanoantennas used in this thesis were fabricated. After the deposition of the nanostructures was complete, the PMMA was lifted off in acetone leaving behind only the metal that was deposited directly on top of the quartz. Heating and low power ultrasonication was used when needed.

3.1.1 Fabrication of 'yang'-shaped nanoantennas

The first set of chiral nanoantennas in this thesis were incomplete circular aluminium nanoantennas, with the main focus to fabricate half-circles with an asymmetry in the thickness of the start and end point (head and tail) - we denote them 'yang'-shaped nanoantennas or simply 'yangs' in this study. These structures are more complex to make than the discs shown in the previous section, due to more parameters to take into account during the fabrication. An example of a sample with fabricated nanoantennas shaped as yangs can be seen in Figure 3.2. In order to fabricate these types of nanoantennas, the mounting stage with the samples had to be tilted during the aluminium deposition. By rotating the tilted sample, a thin circularly shaped line could be deposited. The shape was then determined by the amount of aluminium deposited together with the rotational velocity, resulting in a way of controlling the stop angle of the deposition. An overview of the recipe used in the evaporator can be seen in Appendix A.1.

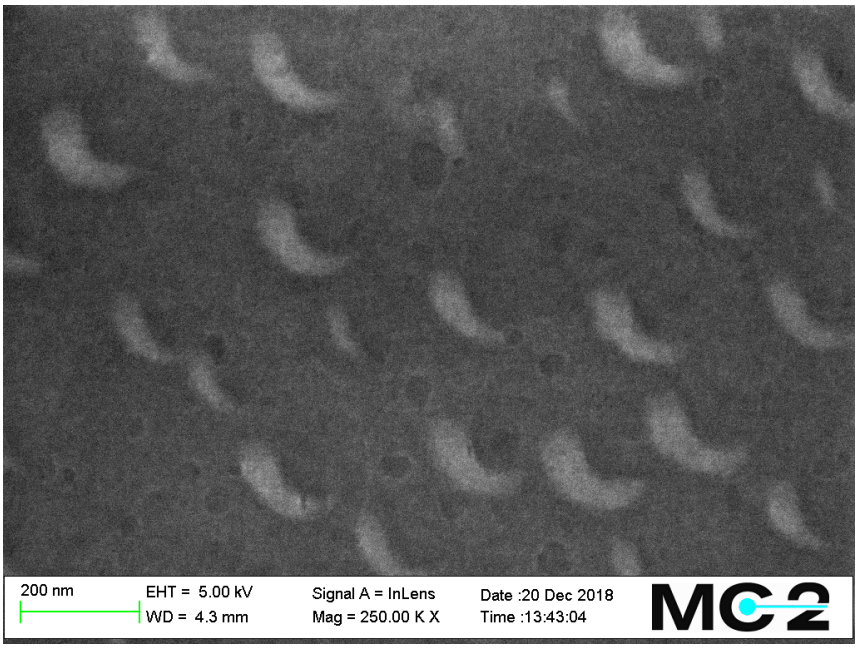

Figure 3.2: SEM micrograph of yang shaped nanoantennas. The chiral asymmetry stems from one end of the half-circles being thicker than the other.

3.1.2 Fabrication of spiral-shaped nanoantennas

Another type of chiral nanoantennas that were fabricated in this thesis, are aluminium spirals. One of the spiral samples can be seen in Figure 3.3. As with the yangs, the mounting stage had to be both tilted and rotated during the aluminium deposition. To not make a circle while rotating, the tilting angle had to change simultaneously resulting in different radii along the spiral. Hence, the final shape was controlled by start and finish tilting angles, tilting velocity, rotational velocity and a stop angle for the rotation. The recipe can be seen in Appendix A.1.

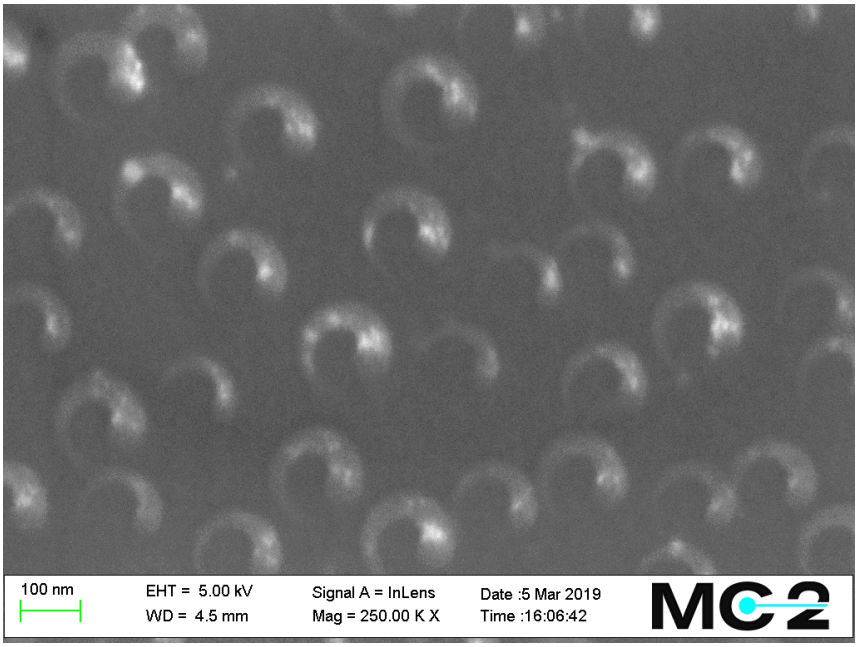

Figure 3.3: SEM micrograph of spiral shaped nanoantennas. The spirals were deposited from the inside out, starting with a thicker head and ending with a thinner tail.

3.2 Optical characterization of samples

In order to characterize the optical properties, conventional optical characterization methods were used to analyze the samples. The measurements included absorption, LD and CD spectroscopy, and aimed at giving an indication of the chiral quality of the samples in order to determine if they would be good candidates for chiral synthesis.

3.2.1 Absorption Spectroscopy

A Varian Cary 50 and an Agilent Cary 60 spectrophotometer (UV-Vis) were used to perform spectroscopic absorption measurements of the samples. White light passes through a monochromator, in which the transmitted wavelength is selected and transmitted. Some of the light travels directly to a reference detector, while most of it is directed towards the sample. A detector behind the sample measures how much of the incoming light that is transmitted through the sample. Due to scattering not being completely negligible for the type of samples fabricated in this thesis, the property measured during the absorption spectroscopy was in fact extinction (i.e. the sum of scattering and absorption). All of the extinction measurements were made with the incoming light being perpendicular to the sample surface, and by letting the monochromator sweep over a wavelength range to obtain an extinction spectrum.

3.2.2 LD and CD Spectroscopy

Measuring the far-field CD of the samples was done using a commercial LD Chirascan machine, capable of measuring LD and CD in both the UV and the visible spectral regions. The LD machine has an isolated sample compartment, and the setup used for the measurements can be seen in Figure 3.4. An iris was used to focus the incoming LD or CD light onto the sample, that was mounted on a rotatory stage. This stage was in turn mounted on a bottom rotatory stage. The two rotatory stages enabled both rotation in plane of the sample, and rotation of the sample holder itself. Mounting of the sample in this manner was necessary, since incoming linearly and circularly polarized light will give rise to different LD and CD spectra depending on how the antennas are rotated in plane. In order to account for inconsistencies in the measurements resulting from this rotational dependence of the CD spectra together with the presence of non-chiral signals leaking into the CD spectra in the form of LD, a method presented by Harada [28] was used. Rotational LD measurements were performed in order to find the maximum LD. The sample was then rotated 45°, corresponding to to the zero (minimum) LD. Then the CD was measured for this angle, before the sample holder was rotated 180° and the CD was measured from the other direction of the sample. By averaging these two CD spectra, the true CD spectrum was obtained.

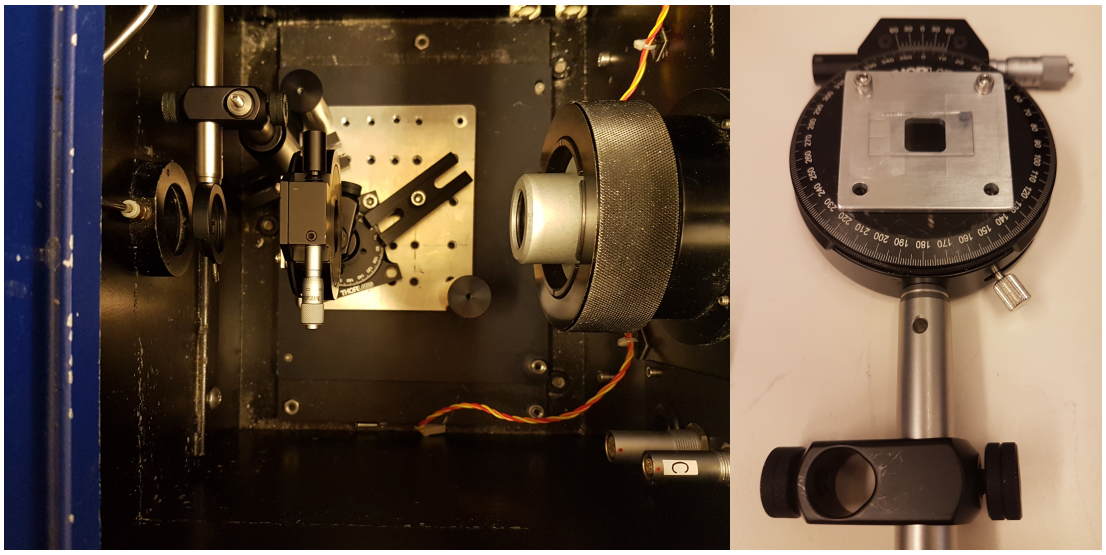

(a) LD machine setup.

(b) Rotatory stage sample holder.

Figure 3.4: Setup used for rotatory LD and CD measurements using the LD machine. The polarized light travels from the left through the iris and sample before reaching the detector to the right. To enable rotation both in plane of the sample and also of the whole sample holder, two rotatory stages were used.

3.3 Imaging techniques

In order to determine the shape, height and distribution of the nanoantennas, they were imaged using scanning electron microscopy (SEM) and atomic force microscopy (AFM).

3.3.1 SEM

The SEM mainly used in this project was a Zeiss Supra 60 VP high vacuum SEM, with a resolution down to a few nm. SEM imaging is done by scanning a conductive surface with a focused electron beam, measuring various signals arising when the electron beam interacts with the sample. Due to the sample surface not being conductive, a conductive polymer (ESpacer) was spin-coated onto the sample surface before imaging. The SEM images were mainly used to give information about the shape and distribution of the nanoantennas.

3.3.2 AFM

AFM was used as a complement to the SEM imaging, mainly to give topographic information about the nanoantennas that the SEM could not provide. The technique is based on scanning probe microscopy (SPM), and the machine used was a Bruker Dimension 3100 SPM. By scanning the surface with a mechanical probe, a topographic image was produced.

3.4 Simulations

The CD of a single nanoantenna has been investigated numerically together with the nanoantenna-enhanced near-fields and its optical chirality distribution around the nanoantenna. These simulations were done using Lumerical, which is a commercial Maxwell solver that we run on the Hebbe supercomputer at Chalmers. The simulations are based on the FDTD (finite-difference time-domain) method, and cover the investigated wavelength range in one simulation run. Parameters gathered from SEM and AFM images were used when building the models in the software, and an example of a yang and a spiral can be seen in Figure 3.5.

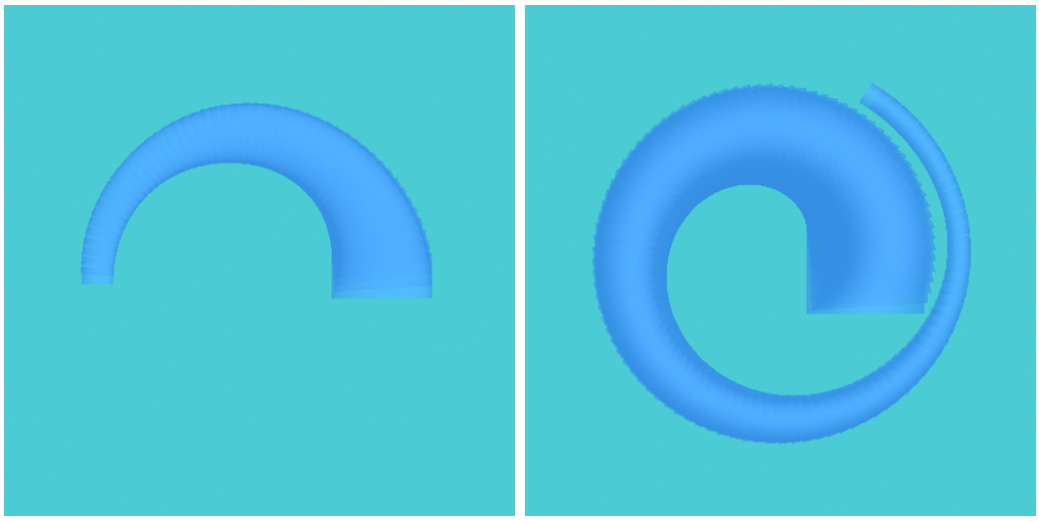

(a) Yang structure used in simulations.

(b) Spiral structure used in simulations.

Figure 3.5: Figures showing yang and spiral structures used in the numerical simulations.

The near-field CD was calculated using the same equation that is used in the CD spectrometers (Equation (2.2)). To obtain the CD spectrum we ran the simulation project separately for the LCP and the RCP light obtaining corresponding transmis-

sion spectra and calculating the CD spectrum from them. The electric and magnetic field components around the nanoantennas were monitored in two planes: the first plane monitor was placed 3 nm above the substrate and the second plane monitor was placed 2 nm above the highest point of the nanoantenna for 50 frequency points (i.e. 50 different wavelengths in the given wavelength span). These field components were then used to visualize the normalized electric near-field, $|\mathbf{E}|/|\mathbf{E_0}|$, and the normalized optical chirality, $|C|/|C_{LCP}|$, which is a property of the electric near-field. The optical chirality C was calculated as described by Schäferling *et al.* [29] and shown in Equation (3.1)

$$C = -\frac{\varepsilon_0 \omega}{2} \mathrm{Im}(\mathbf{E}^* \cdot \mathbf{B}) \tag{3.1}$$

where ε_0 is the electric constant, ω the angular velocity, $\mathbf{E}$ the complex electric field and $\mathbf{B}$ the complex magnetic field. The presented electric fields are normalized by the absolute value of the incident electric field amplitude coming from the source in each simulation. Simulations are run also without the nanostructure present for the chosen circularly polarized light. The optical chirality of a free-propagating circularly polarized light obtained from these runs is used to normalize the optical chirality obtained from the simulations with the nanostructure present. This means that the constants in Equation (3.1) will disappear, and the values shown in the visualizations will hence be showing the change of the optical chirality compared to just illuminating the empty space with either LCP or RCP light. When the absolute value of the ratio $|C|/|C_{LCP}|$ is above 1, the near fields created by the nanoantenna exhibit optical superchirality. An integrated value of the normalized optical chirality of the nanoantenna near-fields is also presented along the optical chirality visualizations. By studying these properties at the wavelengths of interest and comparing them with the experimental data, an indication can be given of whether the nanoantennas can function as selective factors in the chiral synthesis.

3.5 Chiral synthesis

After fabrication and characterization of the samples, the chiral synthesis tests were performed. In short, the DTE-1 molecules were placed in close proximity to the nanoantennas and then they were illuminated from behind with non-polarized light of the desired wavelength. The aim was then for the nanoantennas to transform this into circularly polarized light by their chirality and by the enhanced near-field surrounding them, the isomerization of DTE-1 would result in an enantiomeric excess. This idea is schematically shown in Figure 3.6.

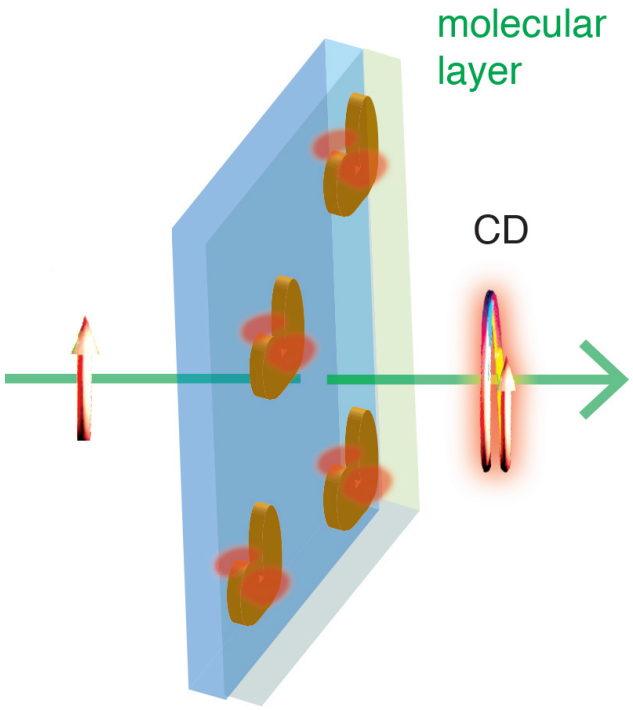

Figure 3.6: Schematic figure showing the method used for the chiral synthesis. The DTE-1 covered samples are illuminated from behind with non-polarized light of either 302 nm or 302 and 523 nm, which is made into circularly polarized light by the nanoantennas. The aim is for the enhanced near-fields to create an enantiomeric excess of the molecules.

First, the DTE-1 molecules had to be placed in direct proximity of the plasmonic chiral nanoantennas to be exposed to the near-fields. The molecular layer had to be thin enough to keep the molecules close to the antennas and the layer also had to contain enough molecules that could be affected by the near-field of the antennas. This was firstly done by spin-coating a molecular film of DTE-1 dissolved in the solvent tetrahydrofuran (THF) and then mixed with PS. During these experiments, the concentrations of the different film components were varied together with the spinning velocities. By doing this, the layers were thin enough but the amount of molecules was too low to detect any changes in the absorption after isomerization and hence too low to detect any CD change. To increase the DTE-1 concentration but keep a low thickness, drop-coating of very high concentrations of DTE-1 in THF was used instead. The solution was left to dry (i.e. letting the THF evaporate), leaving behind a thin layer of highly concentrated DTE-1 molecules.

After applying the molecules, the samples were illuminated from behind with i) 302 nm or ii) 302 and 523 nm for 10 min. The isomerized molecular layers were then washed off with THF in the dark to avoid non-controlled reverse isomerization. Absorption was measured for the washed off solution, and if needed the solution was further diluted before measuring the CD. Figure 3.7 shows an example of the drop-coated DTE-1 after isomerization together with the washed off and diluted

solution of isomerized DTE-1 in THF used for CD measurements.

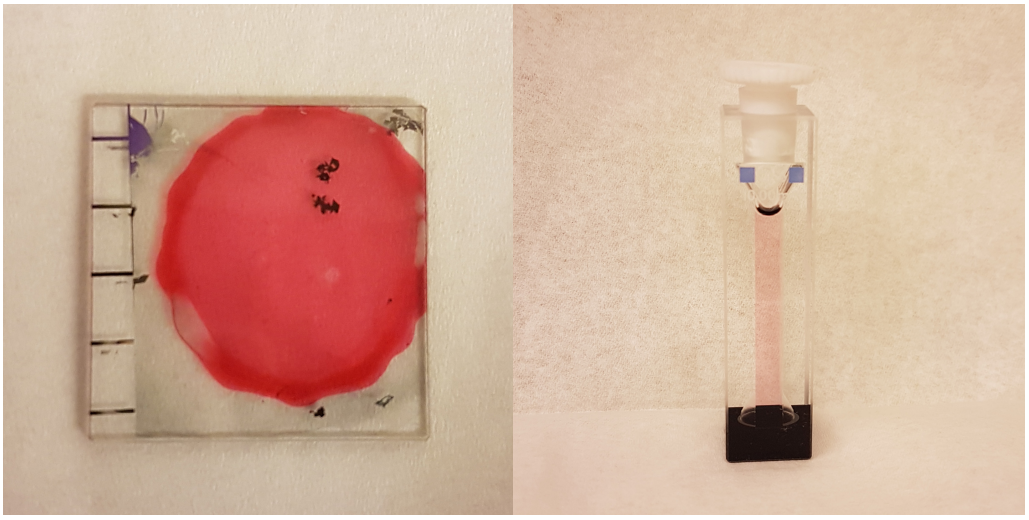

(a) Drop-coated isomerized DTE-1. **(b)** Diluted isomerized DTE-1.

Figure 3.7: Images showing the isomerized DTE-1. The left image shows the drop-coated molecules and the right image shows the diluted DTE-1 in THF used for the CD measurements.

The reason for diluting the washed off solution before measuring the CD, is that too high concentrations of DTE-1 results in an artificial CD signal shown in the CD spectrum obtained from the CD machine. This is due to the absorption of the molecules affecting the CD. Hence, before performing the chiral synthesis a limiting concentration had to be determined. This was done by measuring the CD before and after illuminating the solutions, and then finding the highest DTE-1 concentration that did not give rise to any CD change. It was the absorption spectrum of the isomerized form for this concentration that was used as an upper limit when diluting the washed off solutions after illumination of the molecule covered samples, by comparing the closed form peak. When measuring the CD of the diluted washed off isomerized solutions, the quest was to see if there was a shift of the CD compared to illuminating a drop-coated DTE-1 layer on quartz without any nanoantennas.

4

Results and Discussion

This chapter focuses on the key findings of this thesis. The results are presented and discussed in three main sections: experimental sample characterization, numerical sample characterization and chiral synthesis.

4.1 Experimental sample characterization

When fabricating the plasmonic nanoantennas, the aim was to fabricate chiral structures that could induce an enantiomeric excess of the DTE-1 molecules in the closed form. By controlling the deposition of aluminium when fabricating the nanoantennas, different asymmetric structures could be obtained. Two examples of the fabricated asymmetric structures are yangs and spirals. SEM and AFM images of a yang covered sample can be seen in Figure 4.1, and SEM and AFM images of a spiral covered sample can be seen in Figure 4.2. The PS beads used had an average diameter of 60 nm, but variations in size between the different beads resulted in differently sized nanoantennas as can be seen in the images.

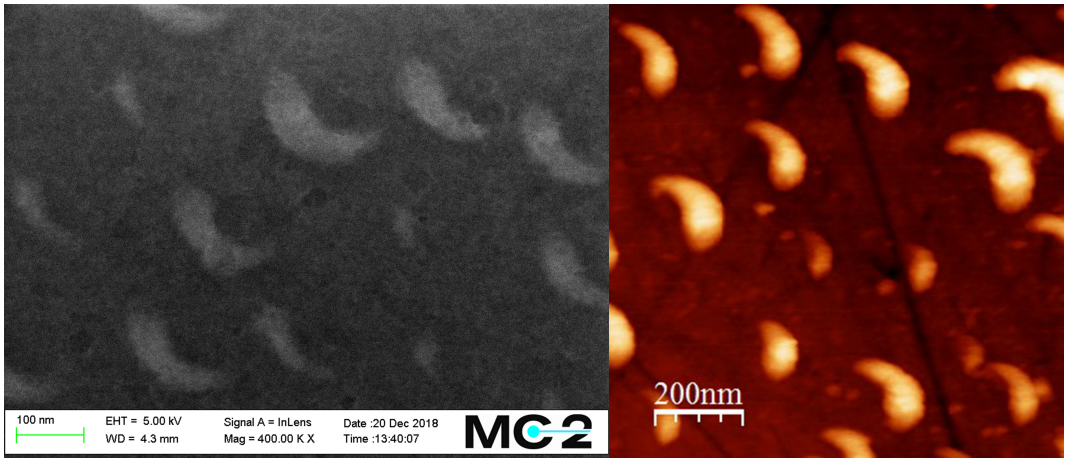

(a) SEM image of yang sample. **(b)** AFM image of yang sample.

Figure 4.1: SEM and AFM images of the fabricated yang samples.

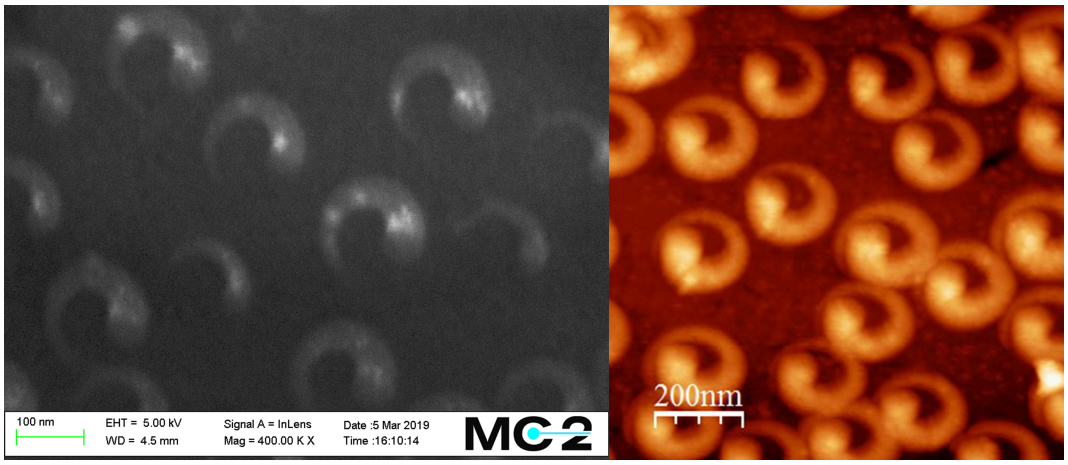

(a) SEM image of spiral sample. **(b)** AFM image of spiral sample.

Figure 4.2: SEM and AFM images of one of the fabricated spiral samples.

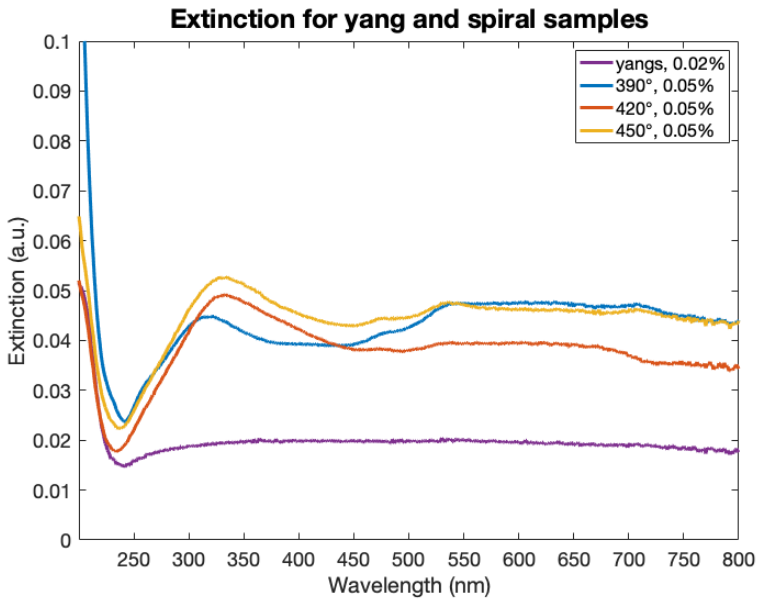

Figure 4.3: Extinction spectra for yang sample (0.02% bead concentration) and spiral samples with stop angles 390°, 420° and 450° (0.05% bead concentration). The extinction is quite low for all samples, but the spirals seems to have small peaks that coincide with the absorption of the open and closed form of the DTE-1 molecules.

The fabricated samples were optically characterized, in order to get an indication if they could function as enantiospecific selectors for chiral synthesis. Figure 4.3 shows the extinction spectra for a yang sample (0.02% bead concentration) and spiral samples with stop angles 390°, 420° and 450° (0.05% bead concentration). All four samples display quite low extinction values over the whole wavelength span, but small peaks that coincide with the absorption of the open and closed form of the DTE-1 molecules can be seen for the three spiral samples. It is not clear how the extinction couples to the CD of the nanoantennas, but an enhanced extinction could be interpreted as a sign of plasmonic enhancement at the desired wavelengths.

Results showing the LD and CD spectra obtained from rotational measurements, with a 45° in plane shift between the measurements can be seen in Figure 4.4 for the spiral sample with stop angle 450°. The maximum LD was found at 15°, corresponding to the minimum LD found by rotating the sample 45° to 60°. This was were the sample holder was rotated 180°, in order to measure the CD from the other direction which was needed in order to calculate the actual CD of the sample. The CD spectra corresponding to the rotational LD spectra can also be seen, and it is evident that the CD varies with the in plane rotation of the sample.

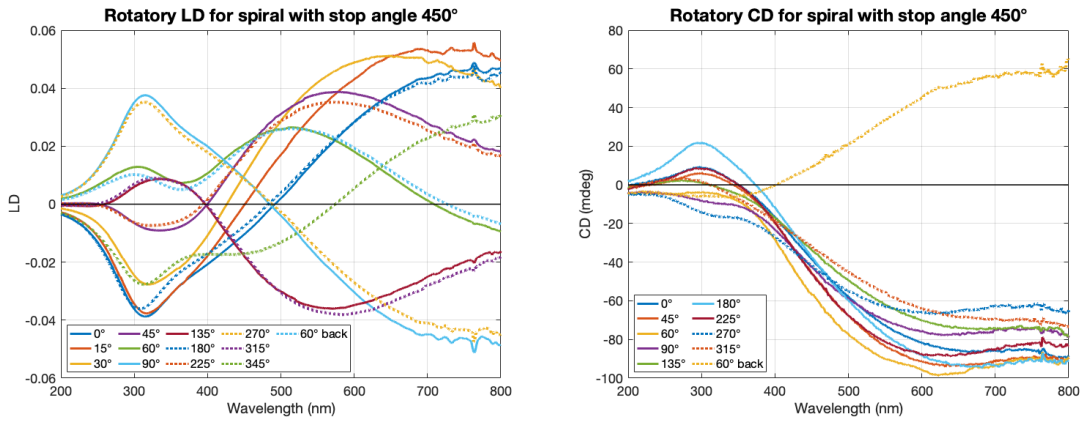

(a) Rotationally measured LD. **(b)** Rotationally measured CD.

Figure 4.4: Rotatory LD and CD spectra for the spiral sample with stop angle 450°. The measurements were made every 45°, in order to find the minimum LD corresponding to 45° more than the maximum LD. In this case, the minimum LD was determined to be at 60° and this was hence were the backside CD measurement was made.

Far-field CD values determined by doing rotational LD and CD measurements for the yang and spiral samples with stop angles 390°, 420° and 450° are shown in Figure 4.5. These spectra can be seen as general indication of whether the plasmonic nanoantennas have an enhanced chiral near-field. The aim was to have indications of an enhanced near-field in the UV around 300 nm and in the visible around 525 nm, since these were the wavelengths of the highest absorption in the open and closed form of the DTE-1 molecules and hence the wavelengths that trigger the isomeriza-

tion. None of the structures show pronounced CD around 300 nm, but from these measurements the yang sample seems to have a slightly stronger CD than the spirals. Around 525 nm, it is the other way around with the spirals showing a lot of CD while the CD of the yang sample is close to zero. There is no real trend visible for the spirals that correlates to an increased stop angle, with especially the 420° spiral sample standing out compared to the other two. This inconsistency could be explained by that the CD does not couple that strongly to this parametric change, or could be due to changes in agglomeration or other inconsistencies between the samples or measurements. More prominent trends could perhaps have been visible if the samples and measurements would have been replicated, which was something that could not be done within the time frame of this thesis.

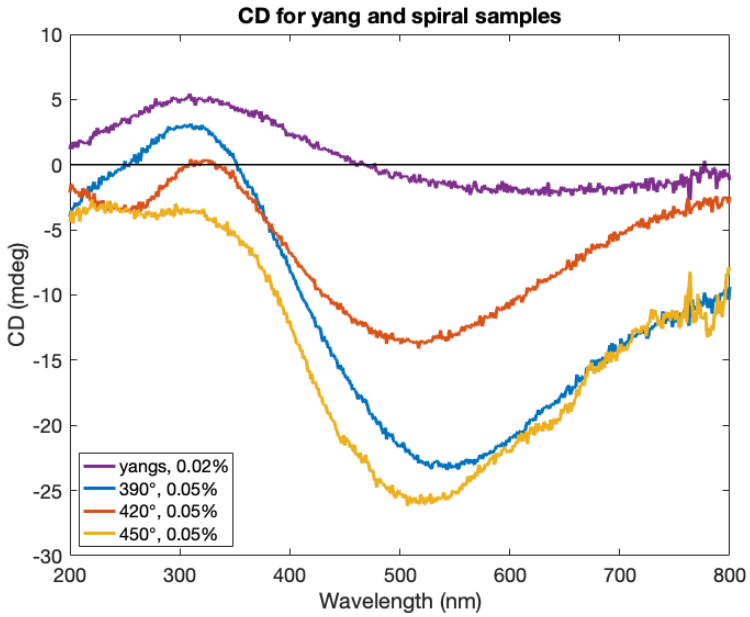

Figure 4.5: Experimentally measured CD spectra for yang sample (0.02% bead concentration) and spiral samples with stop angles 390°, 420° and 450° (0.05% bead concentration). These spectra were determined by doing rotational LD and CD measurements.

4.2 Numerical sample characterization

Another method that was used to get an indication of whether the nanoantennas could function as enantiospecific selectors for the chiral synthesis was numerical simulations of single nanoantennas. These simulations consisted of calculating the nanoantenna-enhanced near-fields and its optical chirality, and functioned as a way of validating and confirming the indications from the experimental far-field CD measurements. Figure 4.6 shows the numerically calculated CD of the yang and three spirals with varying stop angles. Based on these simulations, the CD for the yang is a lot lower than for the spirals over the whole UV-Vis wavelengths region.

All four structures show a shift in the sign of the CD between 300 nm and 400 nm, and the CD of the three spirals is almost identical apart from a slight shift of the 390° spiral between 550 nm and 700 nm.

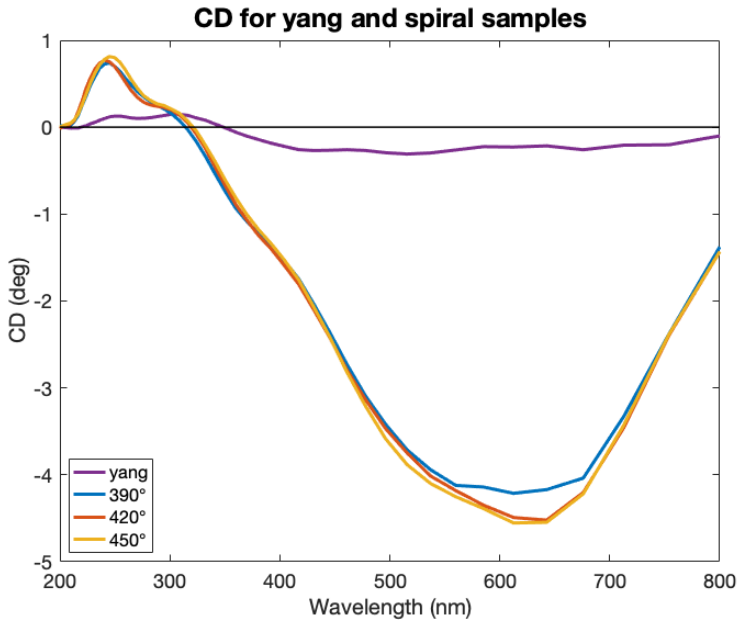

Figure 4.6: Numerically calculated CD spectra for yang and spirals with stop angles 390°, 420° and 450°.

One explanation to why the CD of the three different spirals is so similar in the simulations, could be the presence of computational artifacts arising from how the structures were designed in Lumerical. The main artifact seems to arise from the sharp corners, which is something that can be seen in Figure 4.7 and Figure 4.8. These figures show the electric fields and optical chirality 3 nm above the substrate, and hence cut through the whole structure. Some of the highest values are found close to the corners, which leads to them possibly taking over the effect of changing the stop angle and therefore showing similar results both in the CD and the near-fields of all three spiral nanoantennas. Therefore, all field visualizations presented show the same spiral (the one with stop angle 450°) since the results are very similar for all three.

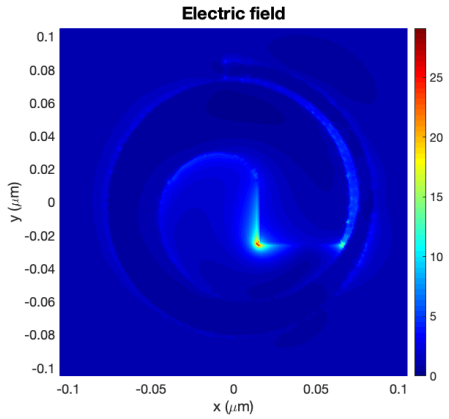

(a) **E** field LCP.

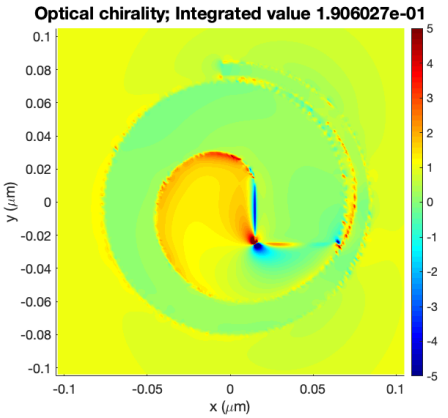

(b) C field LCP.

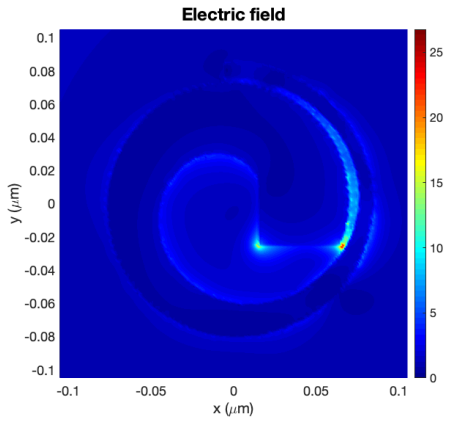

(c) **E** field RCP.

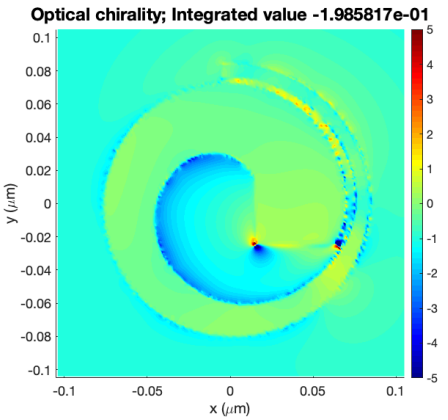

(d) C field RCP.

Figure 4.7: Electric fields and optical chirality in a plane 3 nm above the substrate, visualized at 302 nm for a spiral with stop angle 450°. (a) and (b) show the fields for LCP light, while (c) and (d) show the fields for RCP light. The integrated values of the optical chirality are given with the optical chirality visualizations.

Figure 4.7 shows the electric fields and optical chirality at 302 nm in a plane 3 nm above the substrate. The top two figures display the fields when using a source of LCP light, while the bottom two figures show the fields with an RCP light source. In Figure 4.8, the corresponding figures at 516 nm can be seen. These two wavelengths were chosen, since they corresponded to the two frequency points being closest to the two wavelengths of main interest in this thesis. Apart from the corner effects discussed, it is also clear that there is some field enhancement present around the curved edges of the spiral and between the two parts of the spiral which overlap each other. This indicates that there is some chiral field enhancement arising from the structure that does not seem to stem from computational artifacts as sharp corners. Refining the structures to get rid off these corner effects would give a more definite answer to this, and is something that needs to be done if a more true picture of the near-fields is to be presented.

An integrated value of the optical chirality is presented together with the visualizations, and it is non-zero at both wavelengths. The values in the plane 3 nm above the substrate are fairly similar for both wavelengths but slightly higher at 302 nm. The difference in sign between the LCP and RCP simulations shows that the structures are indeed chiral, since they interact differently with LCP and RCP light.

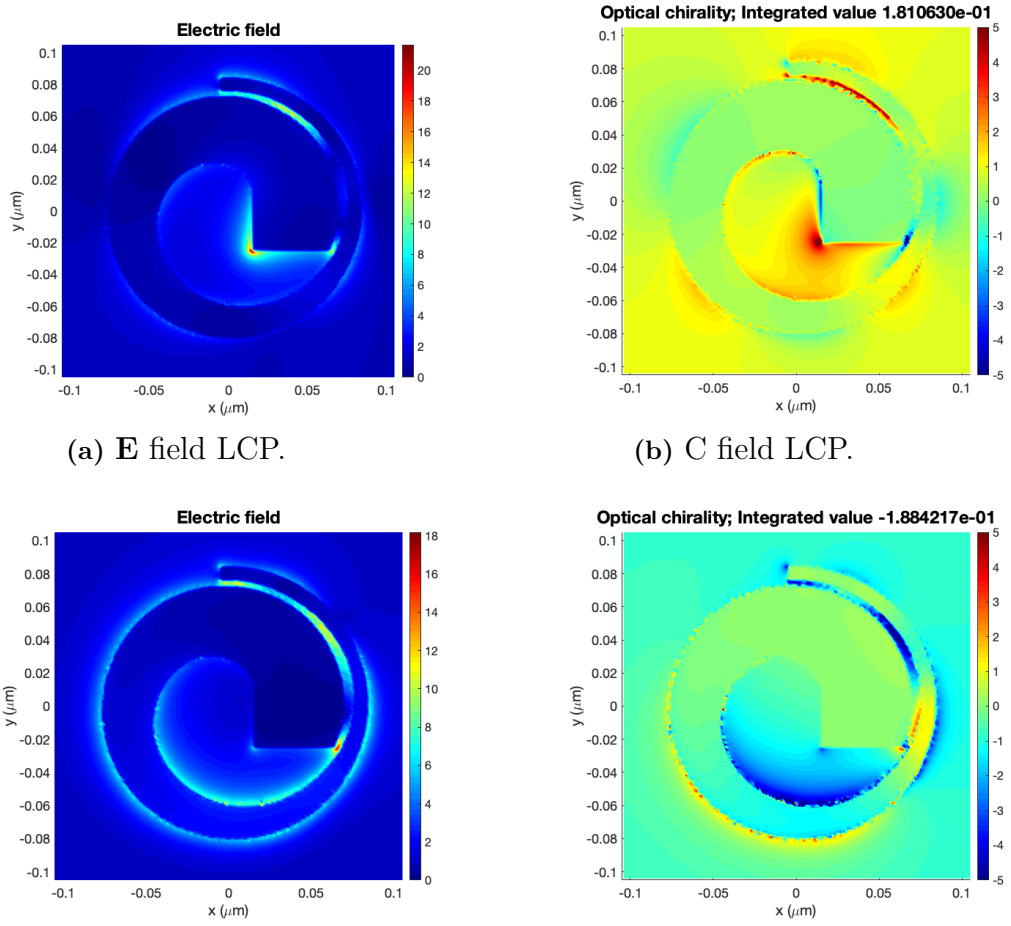

(a) **E** field LCP.

(b) C field LCP.

(c) **E** field RCP.

(d) C field RCP.

Figure 4.8: Electric fields and optical chirality in a plane 3 nm above the substrate, visualized at 516 nm for a spiral with stop angle 450°. (a) and (b) show the fields for LCP light, while (c) and (d) show the fields for RCP light. The integrated values of the optical chirality are given with the optical chirality visualizations.

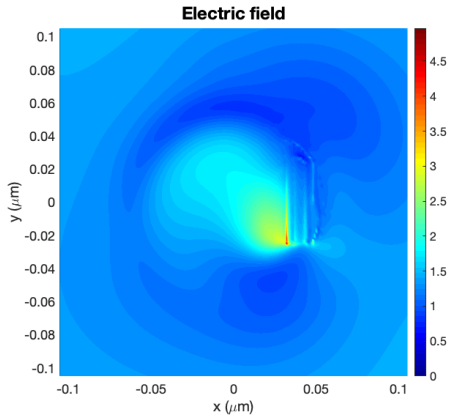

(a) **E** field LCP.

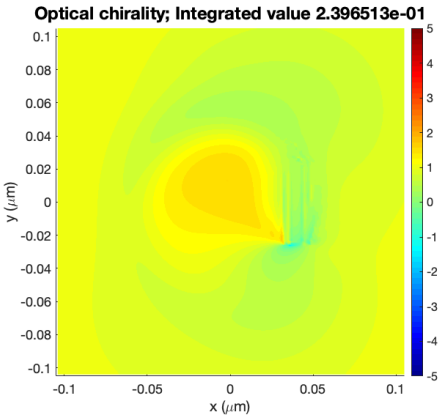

(b) C field LCP.

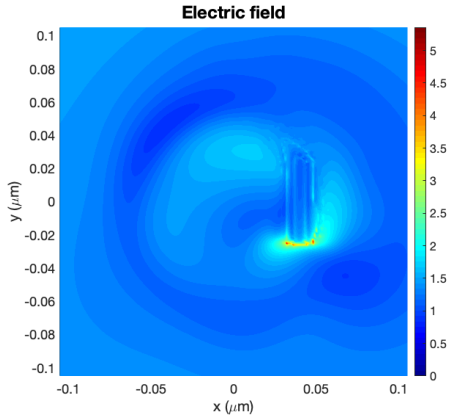

(c) **E** field RCP.

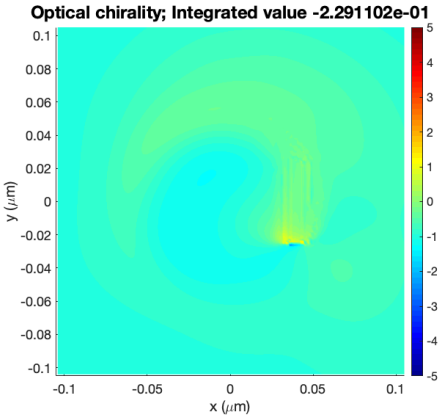

(d) C field RCP.

Figure 4.9: Electric fields and optical chirality in a plane 2 nm above the nanoantenna, visualized at 302 nm for a spiral with stop angle 450°. (a) and (b) show the fields for LCP light, while (c) and (d) show the fields for RCP light. The integrated values of the optical chirality are given with the optical chirality visualizations.

The fields were also monitored and visualized in a plane 2 nm above the highest point of the nanoantenna, and this is shown in Figure 4.9 for 302 nm and Figure 4.10 for 516 nm. In this plane, there are no corners present which would give further indication that the field enhancement is not only caused by computational artifacts. The integrated value of the optical chirality is higher than in the lower plane for both wavelengths, and here the value is higher at 302 nm.

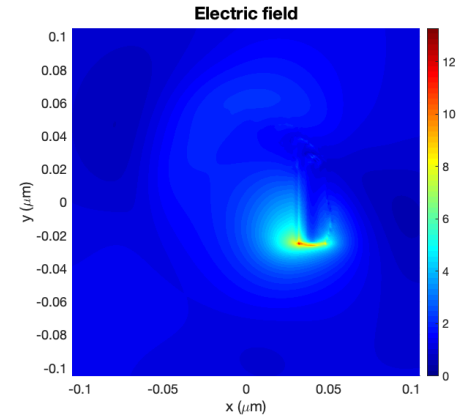

(a) **E** field LCP.

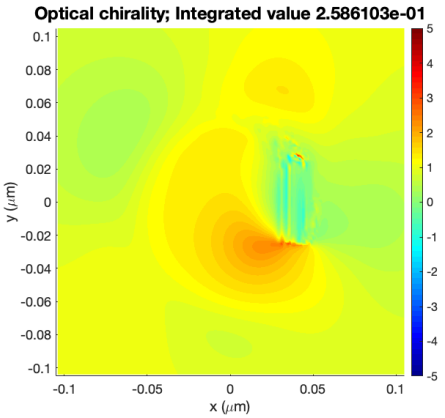

(b) C field LCP.

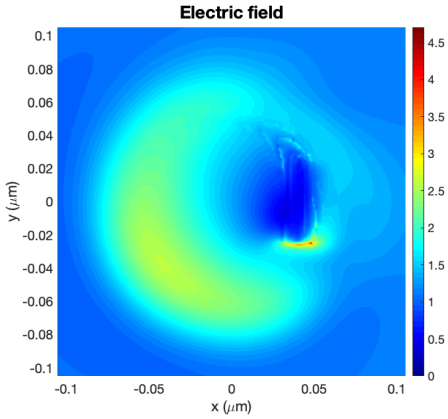

(c) **E** field RCP.

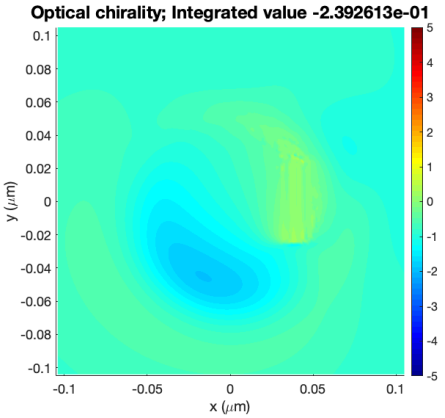

(d) C field RCP.

Figure 4.10: Electric fields and optical chirality in a plane 2 nm above the nanoantenna, visualized at 516 nm for a spiral with stop angle 450°. (a) and (b) show the fields for LCP light, while (c) and (d) show the fields for RCP light. The integrated values of the optical chirality are given with the optical chirality visualizations.

All in all, the simulation results indicate that there seems to be an enhanced chiral near-field close to the nanoantennas that could possibly induce a chiral shift of the photoinduced isomerization of DTE-1 molecules. Since the enhancement seems to be located close to the structures, it is important that the molecules are placed in a close proximity of the nanoantennas in order to ensure that they are properly exposed to the chiral near-fields.

A comparison between the experimentally measured and the numerically calculated CD for the four structures is shown in Figure 4.11. Even if the absolute values of the differently obtained CD spectra differs quite a lot, the shape of the corresponding curves follow the same trend. The differences could be the result of many factors, for example that the experiments were made on samples covered with nanoantennas while the simulations were made on single nanoantennas. The CD obtained in the experimental characterization consisted of a far-field spectra, while the simulations

consist of near-field CD. Computational artifacts could also affect the results obtained from the simulations. The yangs show fairly low CD in the whole spectral region, while the spirals go from low CD in the UV part to high values in the visible part. Both the experimental and numerical characterizations of the structures used in this thesis, give an overall indication that the fabricated samples are chiral and give rise to an enhancement of the chiral near-field around the plasmonic nanoantennas.

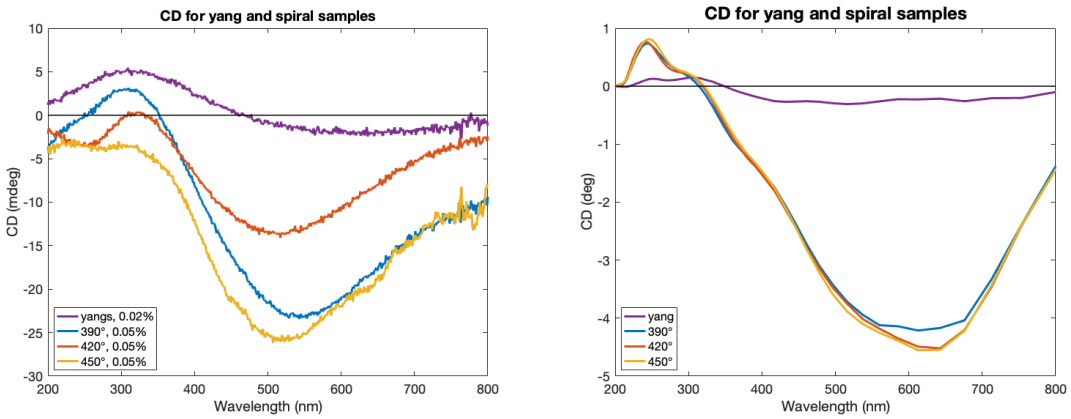

(a) Experimentally measured CD. **(b)** Numerically calculated CD.

Figure 4.11: A comparison between the experimentally measured CD of the fabricated samples and the numerically calculated CD spectra for yang and spirals with stop angles 390°, 420° and 450°. The values of the two CD plots do not coincide very well, but the shape of the corresponding curves are quite similar.

4.3 Chiral synthesis

The experiments testing the chiral synthesis were made in two versions: one when the molecule covered samples were illuminated with 302 nm light for 10 min and one when they were illuminated with light of both 302 nm and 523 nm for 10 min. Both the yang and the three spiral samples were used in the first of these tests, while only the spirals were used in the second test. This was due to a negligibly small CD in the visible region for the yangs according to the previously presented characterization results. While it would have been easier to control and replicate the thickness of the films and hence the concentration of DTE-1 molecules both in the molecular layer and in the washed off solution if it would have worked to use a PS film, the setup used for drop-coating turned out to work well. By using the absorption spectra of the maximum concentration of DTE-1 that could be used for CD measurements without producing an artificial CD, the concentration could be limited during wash off and dilution of the solution. The results from the comparisons of the absorption spectra in the two chiral synthesis tests that were performed can be seen in Figure 4.12, and it is evident that all tested solutions had a lower absorption than the maximum

reference concentration.

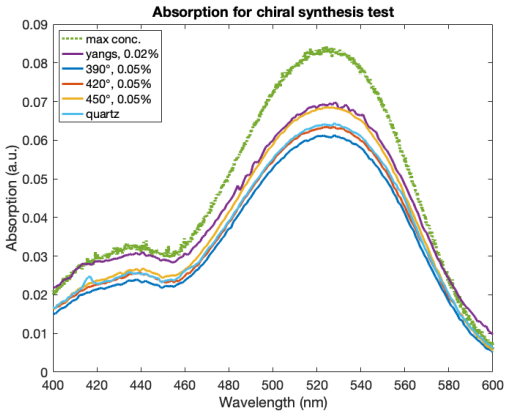

(a) Absorption after 302 nm illumination.

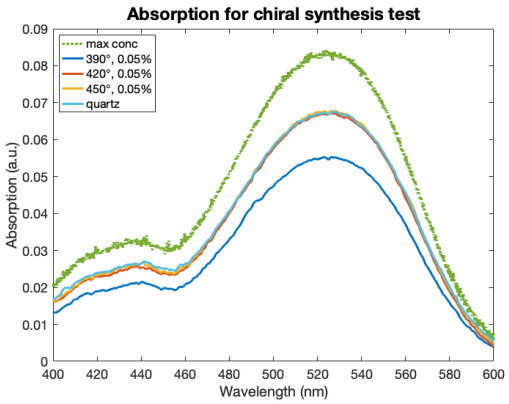

(b) Absorption after 302 nm and 523 nm illumination.

Figure 4.12: Absorption for the washed off and diluted isomerized solutions that were used for CD measurements during the chiral synthesis experiments, compared to the maximum concentration of DTE-1 molecules dissolved in THF that does not give a fake CD in the CD machine. (a) shows absorption for the yang sample (0.02% bead concentration), spiral samples with stop angles 390°, 420° and 450° (0.05% bead concentration) and reference quartz after 10 min illumination with 302 nm light, and (b) shows absorption for the spiral samples with stop angles 390°, 420° and 450° (0.05% bead concentration) and reference quartz after 10 min illumination with 302 and 523 nm light.

Along with the tests being made with the samples covered in nanoantennas, the isomerization tests were also made on quartz as a reference. When presenting the results from the CD measurements of the isomerized solutions, the CD spectra presented show the CD from the structurally induced isomerization minus the CD from the isomerization on quartz. This means that the non-zero CD at certain wavelengths is the CD shift compared to illuminating the DTE-1 molecules without the nanoantennas. Figure 4.13 shows the raw data obtained from both illumination tests, and Figure 4.14 shows the same data after being made smoother in MATLAB using a moving average algorithm. The spectral region of the CD is similar to the absorption of the closed isomer that was shown in Figure 2.5, which was anticipated.

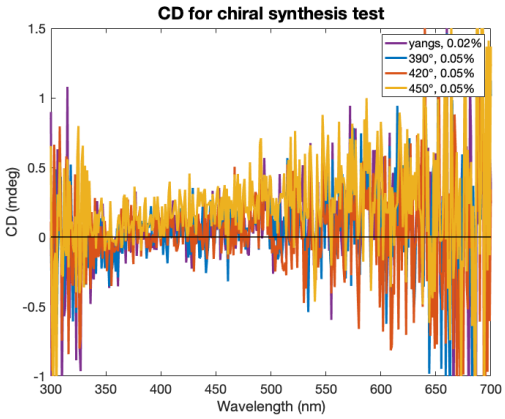

(a) CD after 302 nm illumination.

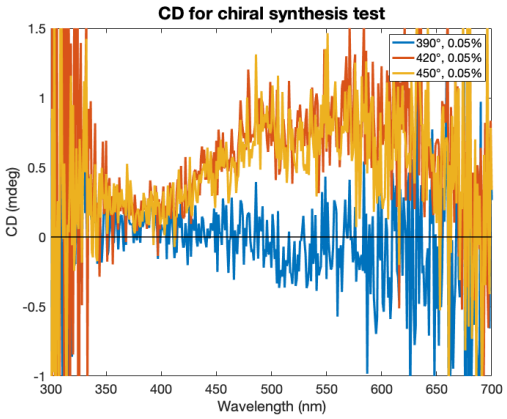

(b) CD after 302 nm and 523 nm illumination.

Figure 4.13: CD for the washed off and diluted isomerized solutions, after removing the CD for the reference quartz sample. Hence, the non-zero CD seen in the spectra is the CD shift compared to illuminating without the chiral nanoantennas. (a) shows CD for the yang sample (0.02% bead concentration) and spiral samples with stop angles 390°, 420° and 450° (0.05% bead concentration) after 10 min illumination with 302 nm light, and (b) shows absorption for the spiral samples with stop angles 390°, 420° and 450° (0.05% bead concentration) after 10 min illumination with 302 and 523 nm light. The obtained CD spectra are very noisy, but a shift of almost 1 mdeg can be seen in (b) for the spirals with stop angles 420° and 450°.

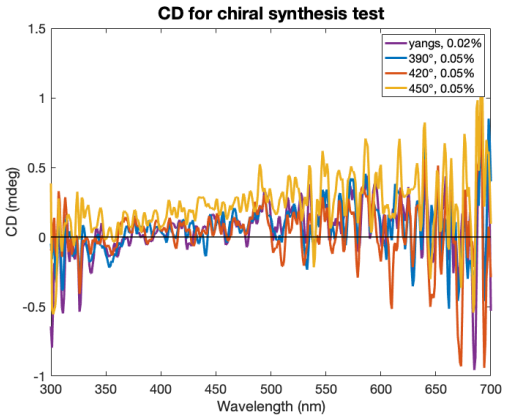

(a) CD after 302 nm illumination.

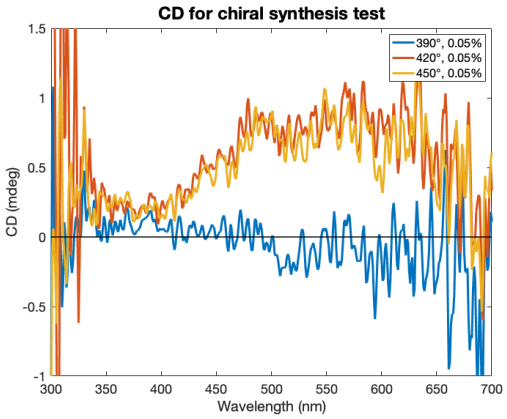

(b) CD after 302 nm and 523 nm illumination.

Figure 4.14: The CD data shown in Figure 4.13 after being made smoother in MATLAB using a moving average algorithm, in order to remove some of the noise in the original plot. The shift in (b) for the spirals with stop angles 420° and 450° is still the most prominent one, but a smaller CD shift for all of the samples in (a) can also be seen.

When only illuminating the samples with 302 nm light, the CD shift is very small with a maximum of around 0.3 mdeg for the spiral sample with stop angle 450° around 550 nm. This CD shift is hard to see, and it is not clear whether there is some sort of correlation between the size of the CD shift and the shape of the nanoantennas. The CD shift was more evident when illuminating the samples with both 302 nm and 523 nm light simultaneously, where a shift of almost 1 mdeg can be seen for the spiral samples with stop angles 420° and 450° around 500 nm to 600 nm. This shift can not be seen for the spiral with stop angle 390°, which instead shows a very small shift to negative CD around the same wavelengths. The reason for the difference between the three spirals is difficult to determine without reproducing the tests, since it could depend both in inconsistencies in the fabrication or handling of the samples but also could have been caused by some inconsistency when performing the chiral synthesis experiments. More tests are also needed in order to determine whether the chiral synthesis that seems to have occurred according to the results is reproducible.

Further modelling of the photochemical reaction that occurs in the vicinity of the chiral plasmonic nanoantennas is needed to determine what happens on a molecular scale, and to explain why the shift seems to be increased when illuminating with both UV and visible light. One explanation to this could be that the chiral nanoantennas create some sort of cycling reaction leading to an enantiomeric excess. Possibly, the nanoantennas create an enantioselective reverse isomerization at 523 nm that results in an enantiomeric excess due to mainly one enantiomer being transformed into the open form. The pumping towards an enantiopure compound would be enhanced if also the original idea of having a chiral enhancement at 302 nm to achieve an enantiomeric excess in the isomerization step from the open to the closed form. One of these phenomena alone would theoretically result in a considerable enantiomeric excess, and combined they have the possibility to be even more effective.

5

Conclusion

This thesis investigated a novel physical approach to nano-optically control a model photochemical reaction, with the aim of obtaining an enantiomeric excess. Large scale samples with plasmonic aluminium nanoantennas of different asymmetric shapes have been fabricated using the fairly simple and versatile nanofabrication method of HCL. Both experimental and numerical characterizations has shown that these samples and nanoantennas seem to have an enhanced chiral near-field at the wavelengths that trigger the forward and reverse isomerization of DTE-1. The shape that displayed the best results in both the experimental and numerical characterizations were spirals, and although the results were not quantitatively comparable they correlated quite well regarding the shape of the CD spectra. The inconsistencies between the results from experiments and simulations were also somewhat expected, since the experiments were made on samples covered in nanoantennas while the simulations were made on single nanoantennas. Also some computational artifacts were present in the simulations, due to some simplifications of the designed structure compared to the fabricated ones.

Chiral synthesis tests that were executed in this thesis indicate that the fabricated chiral plasmonic nanoantennas can be used to achieve an enantiomeric excess in the closed form of DTE-1 for some of the structure. The most prominent results were achieved for two of the spiral samples when illuminating the molecule covered samples with non-polarized light of both 302 nm and 523 nm. Further characterizations and tests with these structures and fabrication using the same parameters will need to be performed in order to determine the reproducibility of the presented results, but this could not be done within the time frame of this thesis.

Some advantages of using the approach presented in this thesis is that plasmonic enhancement has broader peaks than the absorption of the photochromic molecules, resulting in that the enhanced near-field around the nanoantennas can enhance LCP or RCP light in a broad wavelength span. Together with a versatile nanofabrication method, this makes it possible to tune the nanoantennas to match different photochemical systems. Another advantage is that the CD shift indicating an enantiomeric excess could be seen after just 10 min of illumination, making it a rather quick method. Something that also makes this approach stand out, is that the enantiomeric excess induced by an enhanced chiral near-field is created when using

non-polarized light. Hence, all of the CD shift emerge from the work done by the nanoantennas without the need for having a circularly polarized light source.

In conclusion, this thesis has presented results that could pave the way for a novel physical approach of obtaining enantiopure compounds of model photoswitches. The tests and structures need to be re-done in order to confirm that these findings are reproducible and to fully determine the factors that make this nano-optical control of chiral photochemistry possible. Further work is needed before this approach could be applicable in for example the pharmaceutically-relevant synthesis, but this thesis makes up one step towards this vision.

5.1 Future outlook

The work in this thesis has been part of an ongoing research project. Firstly, the samples and tests presented in the thesis would need to be reproduced in order to confirm the findings and draw further conclusion from the results. The next step, that is already being pursued, is to introduce different materials like gold and silver to try to further enhance the chiral enhancement in the visible part of the spectra and also to try to combine these materials with aluminium. By fabricating and testing nanostructures with varying chiral enhancement in both the UV and the visible spectral regions, the role of the chiral plasmonic nanoantennas would become more clear. Systematic tests regarding the chiral synthesis would also be of interest, where parameters like illumination time and perhaps polarized light sources could be studied. A further goal is to combine noble metals and metallic ferromagnetic elements, to enable modification of the optical near-field of such nanoantennas by externally applied milli-Tesla magnetic fields. This would mean that the plasmonic properties, and hence the chiral synthesis, would be controlled by magnetic fields.

References

[1] N. Chhabra, M. L. Aseri, and D. Padmanabhan, "A review of drug isomerism and its significance," *International Journal of Applied and Basic Medical Research*, vol. 3, no. 1, pp. 16–18, 2013.

[2] I. Zubritskaya, "Designer magnetoplasmonics for adaptive nano-optics," Ph.D. dissertation, University of Gothenburg, SE-412 96 Gothenburg, 2017.

[3] L. A. Nguyen, H. He, and C. Pham-Huy, "Chiral Drugs: An Overview," *International Journal of Biomedical Science*, vol. 2, no. 2, pp. 85–100, 2006.

[4] M. L. Solomon, J. Hu, M. Lawrence, A. García-Etxarri, and J. A. Dionne, "Enantiospecific Optical Enhancement of Chiral Sensing and Separation with Dielectric Metasurfaces," *ACS Photonics*, vol. 6, no. 1, pp. 43–49, 2019.

[5] T. C. S. Pace, V. Müller, S. Li, P. Lincoln, and J. Andréasson, "Enantioselective Cyclization of Photochromic Dithienylethenes Bound to DNA," *Angewandte Chemie International Edition*, vol. 52, no. 16, pp. 4393–4396, 2013.

[6] H. Fredriksson, Y. Alaverdyan, A. Dmitriev, C. Langhammer, D. S. Sutherland, M. Zäch, and B. Kasemo, "Hole-Mask Colloidal Lithography," *Advanced Materials*, vol. 19, no. 23, pp. 4297–4302, 2007.

[7] S. A. Maier, *Plasmonics: Fundamentals and Applications.* Springer, 2007.

[8] L. Novotny and B. Hecht, *Principles of Nano-Optics.* Cambridge University Press, 2006.

[9] S. V. Gaponenko, *Introduction to Nanophotonics.* Cambridge University Press, 2010.

[10] M. F. Ashby, P. J. Ferreira, and D. L. Schodek, *Nanomaterials, Nanotechnology and Design - An Introduction for Engineers and Architects.* Elsevier, 2009.

[11] "The Lycurgus Cup," The British Museum - Collection online [online] Available at:

https://www.britishmuseum.org/research/collection_online/collection_object_details.aspx?assetId=36154001&objectId=61219&partId=1 [Accessed 2019–05–13].

[12] W. L. Barnes, A. Dereux, and T. W. Ebbesen, "Surface plasmon subwavelength optics," *Nature*, vol. 424, pp. 824–830, 2003.

[13] J. M. Luther, P. K. Jain, T. Ewers, and A. P. Alivisatos, "Localized surface plasmon resonances arising from free carriers in doped quantum dots," *Nature Materials*, vol. 10, pp. 361–366, 2011.

[14] D. Gérard and S. K. Gray, "Aluminium plasmonics," *Journal of Physics D: Applied Physics*, vol. 48, no. 18, 2014.

[15] M. W. Knight, N. S. King, L. Liu, H. O. Everitt, P. Nordlander, and N. J. Halas, "Aluminium for plasmonics," *ACS Nano*, vol. 8, no. 1, pp. 834–840, 2014.

[16] R. Janoschek, *Chirality - From Weak Bosons to the α-Helix*. Springer, 1991.

[17] "What is chirality?" Khan Academy on Chiral Drugs [online] Available at: https://www.khanacademy.org/test-prep/mcat/chemical-processes/stereochemistry/a/chiral-drugs [Accessed 2019–05–14].

[18] E. Hecht, *Optics*, 4th ed. Pearson, 2014.

[19] "Circular Polarization Circularly Polarized Light Without Components Right Handed," by Dave3457 - Own work, Public Domain [online] Available at: https://commons.wikimedia.org/w/index.php?curid=9861553 [Accessed 2019–05–14].

[20] X. Wang and Z. Tang, "Circular Dichroism Studies on Plasmonic Nanostructures," *Small*, vol. 13, no. 1, 2016.

[21] M. Irie, T. Fukaminato, K. Matsuda, and S. Kobatake, "Photochromism of Diarylethene Molecules and Crystals: Memories, Switches, and Actuators," *Chemical Reviews*, vol. 114, no. 24, pp. 12 174–12 277, 2014.

[22] M. Irie, "Diarylethenes for Memories and Switches," *Chemical Reviews*, vol. 100, no. 5, pp. 1685–1716, 2000.

[23] B. M. Maoz, Y. Chaikin, A. B. Tesler, O. Bar Elli, Z. Fan, A. O. Govorov, and G. Markovich, "Amplification of Chiroptical Activity of Chiral Biomolecules by Surface Plasmons," *Nano Letters*, vol. 13, no. 3, pp. 1203–1209, 2013.

[24] V. K. Valev, J. J. Baumberg, C. Sibilia, and T. Verbiest, "Chirality and Chiroptical Effects in Plasmonic Nanostructures: Fundamentals, Recent Progress,

and Outlook," *Advanced Materials*, vol. 25, no. 18, pp. 2517–2534, 2013.

[25] M. Hentschel, M. Schäferling, X. Duan, H. Giessen, and N. Liu, "Chiral Plasmonics," *Science Advances*, vol. 3, no. 5, 2017.

[26] J. G. Gibbs, A. G. Mark, S. Eslami, and P. Fischer, "Plasmonic nanohelix metamaterials with tailorable giant circular dichroism," *Applied Physics Letters*, vol. 103, no. 21, pp. 10–14, 2013.

[27] C. Song, M. G. Blaber, G. Zhao, P. Zhang, H. C. Fry, G. C. Schatz, and N. L. Rosi, "Tailorable Plasmonic Circular Dichroism Properties of Helical Nanoparticle Superstructures," *Nano Letters*, vol. 13, no. 7, pp. 3256–3261, 2013.

[28] T. Harada, "Application of a polarized modulation technique in supramolecular science: chiroptical measurements of optically anisotropic systems," *Polymer Journal*, vol. 50, no. 8, pp. 679–687, 2018.

[29] M. Schäferling, X. Yin, N. Engheta, and H. Giessen, "Helical Plasmonic Nanostructures as Prototypical Chiral Near-Field Sources," *ACS Photonics*, vol. 1, no. 6, pp. 530–537, 2014.

A

Appendix

A.1 Lesker PVD 225 #2 recipes for yangs and spirals

The recipe used in Lesker PVD 225 #2 for the fabrication of yang shaped nanoantennas is shown in Figure A.1, and is called *R TR Al*. During the yang fabrication, the parameters shown in the recipe were used: 4. Platen Motor Position Set Point (tilt angle) was $-10°$, 7. Planet Motor Jog Velocity SP (rotational velocity) was 0.1 rpm and together with the total deposited thickness of 60 nm these parameters resulted in yangs.

Figure A.2 shows recipe *R TR Al Slow rot + tilt + stop at angle*, which was used for fabrication of spirals. During the spiral fabrication, some of the parameters shown were the same for all three spirals: 4. Platen Motor Position Set Point (initial tilt angle) was $-10°$, 8. Planet Motor Jog Velocity SP (rotational velocity) was 0.2 rpm, 18. Platen Motor Position Set Point was $-20°$, 19. Platen Motor Position Velocity SP (tilting velocity) was 0.005, 24. Planet Motor Position (check angle less than 360° to enable rotation of more than 360°) was 350° and 25. Dwell (dwelling time to enable rotation of more than 360°) was 15 s. The parameter that was changed between the different spirals was: , 26. Planet Motor Position (stop angle) was 30° for 390° spiral, 60° for 420° spiral and 90° for 450° spiral.

Recipe Name	Order	Equipment	Equipment Ref	Operation	Value
R TR Al	1	Recipe	Set Abort Recipe	Abort Process	
	2	Recording	Start Recording	Start	
	3	Recipe	Run Recipe	0 tilt rotation	
	4	Motors	Platen Motor Position Set Point	Set Value = n.nn	-10
	5	Motors	Platen Motor Go To Position	Turn_On/Open/Opening	
	6	Gauge	MKS979 WRG Pressure	Check Value <= n.nn	0.0000005
	7	Motors	Planet Motor Jog Velocity SP	Set Value = n.nn	0.1
	8	Motors	Planet Motor Go Continuous +	Turn_On/Open/Opening	
	9	Recipe	Run Recipe	Set shutter mapping	
	10	Shutter	Substrate Shutter	Turn_Off/Closed/Closing	
	11	Recipe	Run Recipe	Initialize recipe load	
	12	Sigma	Sigma Control Request	Set Value = n.nn	R Al
	13	Sigma	Sigma Load Process	Turn_On/Open/Opening	
	14	Sigma	Sigma Process Name	Compare String Value =	R Al
	15	Recipe	Run Recipe	Select Al	
	16	Recipe	Run Recipe	E-gun ON	
	17	Recipe	Run Recipe	Start Process	
	18	Recipe	Run Recipe	Wait for Process stopped	
	19	Motors	Planet Motor Go Continuous +	Turn_Off/Closed/Closing	
	20	Recipe	Run Recipe	E-gun OFF	
	21	Shutter	Ebeam Shutter	Turn_Off/Closed/Closing	
	22	Recipe	Run Recipe	0 tilt rotation	
	23	Recording	Start Recording	Stop	

Figure A.1: Recipe R TR Al used for fabrication of yangs.

Recipe Name	Order	Equipment	Equipment Ref	Operation	Value
R TR Al Slow rot + tilt + stop at angle	1	Recipe	Set Abort Recipe	Abort Process	
	2	Recording	Start Recording	Start	
	3	Recipe	Run Recipe	0 tilt rotation	
	4	Motors	Platen Motor Position Set Point	Set Value = n.nn	-10
	5	Motors	Platen Motor Go To Position	Turn_On/Open/Opening	
	6	Recipe	Run Recipe	Rotate to 0	
	7	Gauge	MKS979 WRG Pressure	Check Value <= n.nn	0.0000005
	8	Motors	Planet Motor Jog Velocity SP	Set Value = n.nn	0.2
	9	Recipe	Run Recipe	Set NO shutter mapping	
	10	Shutter	Substrate Shutter	Turn_Off/Closed/Closing	
	11	Recipe	Run Recipe	Initialize recipe load	
	12	Sigma	Sigma Control Request	Set Value = n.nn	R Al
	13	Sigma	Sigma Load Process	Turn_On/Open/Opening	
	14	Sigma	Sigma Process Name	Compare String Value =	R Al
	15	Recipe	Run Recipe	Select Al	
	16	Recipe	Run Recipe	E-gun ON	
	17	Recipe	Run Recipe	Start Process	
	18	Motors	Platen Motor Position Set Point	Set Value = n.nn	-20
	19	Motors	Platen Motor Position Velocity SP	Set Value = n.nn	0.005
	20	Sigma	Sigma Process State	Compare String Value =	Deposit
	21	Recipe	Run Recipe	Shutter OPEN	
	22	Motors	Planet Motor Go Continuous +	Turn_On/Open/Opening	
	23	Motors	Platen Motor Go To Position	Turn_On/Open/Opening	
	24	Motors	Planet Motor Position	Check Value > n.nn	350
	25	Recipe	Dwell	N Seconds (n or HH:MM:SS)	15
	26	Motors	Planet Motor Position	Check Value > n.nn	90
	27	Shutter	Substrate Shutter	Turn_Off/Closed/Closing	
	28	Recipe	Run Recipe	Wait for Process stopped	
	29	Motors	Planet Motor Go Continuous +	Turn_Off/Closed/Closing	
	30	Motors	Platen Motor Position Velocity SP	Set Value = n.nn	1
	31	Recipe	Run Recipe	E-gun OFF	
	32	Shutter	Ebeam Shutter	Turn_Off/Closed/Closing	
	33	Recipe	Run Recipe	0 tilt rotation	
	34	Recording	Start Recording	Stop	

Figure A.2: Recipe R TR Al Slow rot + tilt + stop at angle used for fabrication of spirals.